

# FROSTBYTE: A reproducible data-driven workflow for probabilistic seasonal streamflow forecasting in snow-fed river basins across North America

Louise Arnal<sup>1,a</sup>, Martyn P. Clark<sup>1,2</sup>, Alain Pietroniro<sup>2</sup>, Vincent Vionnet<sup>3</sup>, David R. Casson<sup>2</sup>, Paul H. Whitfield<sup>1</sup>, Vincent Fortin<sup>3</sup>, Andrew W. Wood<sup>4,5</sup>, Wouter J. M. Knoben<sup>2</sup>, Brandi W. Newton<sup>6</sup>, and Colleen Walford<sup>7</sup>

<sup>1</sup>University of Saskatchewan, Centre for Hydrology, Coldwater Laboratory, Canmore, AB, Canada

<sup>2</sup>Department of Civil Engineering, University of Calgary, Calgary, AB, Canada

<sup>3</sup>Meteorological Research Division, Environment and Climate Change Canada, Dorval, QC, Canada

<sup>4</sup>National Center for Atmospheric Research, Boulder, CO, USA

<sup>5</sup>Colorado School of Mines, Golden, CO, USA

<sup>6</sup>Airshed and Watershed Stewardship Branch, Alberta Environment and Protected Areas, Calgary, AB, Canada

<sup>7</sup>Alberta River Forecast Center, Environment and Protected Areas, Government of Alberta, Edmonton, AB, Canada

<sup>a</sup>now at: Ouranos, Montréal, Québec, Canada

**Correspondence:** Louise Arnal (louise.arnal@usask.ca)

**Abstract.** Seasonal streamflow forecasts provide key information for decision-making in sectors such as water supply management, hydropower generation, and irrigation scheduling. The predictability of streamflow on seasonal timescales relies heavily on initial hydrological conditions, such as the presence of snow and the availability of soil moisture. In high-latitude and high-altitude headwater basins in North America, snowmelt serves as the primary source of runoff generation. This study presents and evaluates a data-driven workflow for probabilistic seasonal streamflow forecasting in snow-fed river basins across North America (Canada and the USA). The workflow employs snow water equivalent (SWE) measurements as predictors and streamflow observations as predictands. Gap filling of SWE datasets is accomplished using quantile mapping from neighboring SWE and precipitation stations, and Principal Component Analysis is used to identify independent predictor components. These components are then utilized in a regression model to generate ensemble hindcasts of streamflow volumes for 75 nival basins with limited regulation from 1979 to 2021, encompassing diverse geographies and climates. Using a hindcast evaluation approach that is user-oriented provides key insights for snow monitoring experts, forecasters, decision-makers, and workflow developers. The analysis presented here unveils a wide spectrum of predictability and offers a glimpse into potential future changes in predictability. Late-season snowpack emerges as a key factor for predicting spring/summer volumes, while high precipitation during the target period presents challenges to forecast skill and streamflow predictability. Notably, we can predict lower and higher than normal streamflows during the spring to early summer with up to five months lead time in some basins. Our workflow is available on GitHub as a collection of Jupyter Notebooks, facilitating broader applications in cold regions and contributing to the ongoing advancement of methodologies.

## 1 Introduction

Seasonal streamflow forecasts play an important role in various sectors, including water supply management, hydropower generation, and irrigation scheduling. It can also provide early warning of floods and droughts. Around the globe, a diverse range of predictors plays a crucial role in seasonal streamflow forecasting. This includes antecedent hydrological conditions (e.g., snowpack, past streamflow, soil moisture) and future conditions (e.g., future precipitation, climate signals). See Yuan et al. (2015) for a comprehensive review of the dominant sources of seasonal hydrological predictability. Various forecasting methods leverage these predictors and hydrological processes that drive streamflow variability in regions of interest.

In Canada and much of the USA, snowmelt is an important driver of streamflow. In spring, the snow accumulated during winter serves as a substantial water reservoir in high-altitude mountainous regions, often referred to as "water towers" (Viviroli et al., 2007). Gradually, this natural water storage releases its stored contents downstream to the rivers through the process of snowmelt. In the western USA, operational seasonal hydrological forecasting relies on the long-term predictability provided by winter snow conditions (Wood et al., 2016). This important natural water supply is however threatened by climate change. Immerzeel et al. (2020) assessed the vulnerability of the world's water towers and found that in North America, vulnerabilities are associated with both population growth and rising temperatures. By understanding the predictability of streamflow originating from snowmelt, we can better address the challenges posed by climate change and effectively manage these invaluable water sources for the future.

Over the past few decades, significant advances have been made in our understanding of forecast quality and hydro-meteorological predictability on seasonal timescales. These have been facilitated, in part, by the continuous improvements in technological capabilities. As a result, a wide range of approaches now exists for streamflow forecasting on seasonal timescales, including process-based, data-driven, and hybrid models, each possessing distinct advantages and limitations (Slater et al., 2023). This paper focuses on data-driven approaches.

Data-driven forecasting involves predicting a variable of interest (known as predictand; e.g., streamflow spring volume) by establishing relationships between the predictand and one or more predictors (e.g., snowpack, past streamflow, climate signals). Various techniques can be employed to model these relationships, ranging from simple linear regressions to more complex machine learning (ML) and/or artificial intelligence (AI) methods. Consider the following noteworthy data-driven approaches for seasonal streamflow forecasting: i) Principal Component Regressions (PCR) have proven effective in streamflow volume forecasting in the USA (Garen, David C., 1992; Mendoza et al., 2017; Fleming and Garen, 2022); ii) Bayesian joint probability statistical modelling has demonstrated its capability for ensemble seasonal streamflow forecasting in Australia (Wang et al., 2009); iii) Seven different Generalized Additive Models for Location, Scale and Shape statistical models were tested to forecast quantiles of seasonal streamflow in the Midwest USA, using a range of predictors such as precipitation, temperature, agricultural land cover and population (Slater and Villarini, 2017); iv) A robust M-regression model was first tested for hydrological forecasting for ensemble seasonal streamflow forecasting in the South Saskatchewan River Basin (Canada), extending the operational forecast lead time by up to two months (Gobena and Gan, 2009); v) Regression models were applied for winter and early spring streamflow forecasting in large North American river basins in Canada and the USA, based on

snowpack information (Dyer, 2008); vi) ~~Machine learning (ML)/artificial intelligence (AI)~~ is now increasingly explored for this type of application. Fleming et al. (2021) explored the use of AI for forecasting of water supplies in the western USA. They showed that it meets the quality and technical feasibility requirements for operational adoption at the US Department of  
55 Agriculture Natural Resources Conservation Service (NRCS).

This work builds on the literature and addresses research gaps by extending the spatial domain of previous studies to include both Canada and the USA. In this work, we use **Principal Component Regressions (PCR)** to predict future streamflow from snow water equivalent (SWE) information as the sole predictor given its importance for seasonal streamflow prediction. PCR stands as a well-established and widely used data-driven method, as demonstrated by the non-exhaustive list above. Simple  
60 statistical regression methods such as PCR offer several key advantages, including their local applicability, intuitive nature (i.e., use of local data to represent known and observed hydrological processes locally), speed and low computational resource requirements. These methods are additionally straightforward to implement and potentially highly reliable.

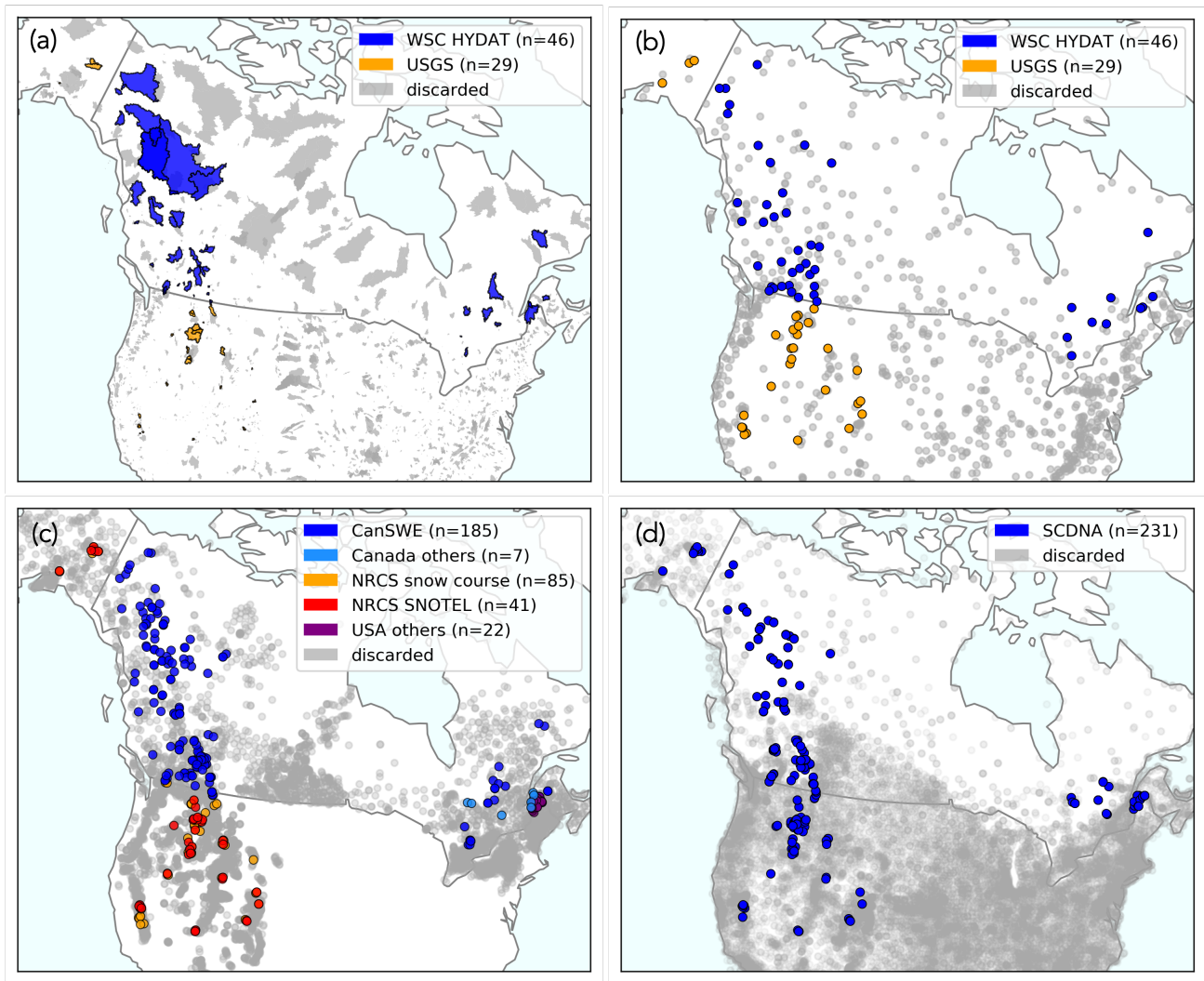
Mendoza et al. (2017) showed that increasing methodological complexity (in their study this was defined as the gradient from purely data-driven techniques to the use of process-based models) does not always lead to improved forecasts. Empha-  
65 sizing simplicity in modeling provides a robust foundation for enhancing our comprehension of hydrological processes and supports ongoing improvements to forecast quality (including through model developments and the use of new observations), as highlighted by Delgado-Ramos and Hervas-Gamez (2018). This approach additionally supports reproducibility to enable collaborative advancements through open science practices (Knoben et al., 2022).

In this paper, we present a reproducible data-driven workflow designed for probabilistic streamflow forecasting in nival  
70 (i.e., snowmelt-driven) river basins across Canada and the USA (Section 2.2). For the sake of simplicity, we use the term 'North America' to refer to the forecasting domain used in this study. Through the analysis of the hindcasts produced with this workflow, we address the research question: can **snow water equivalent (SWE)** be used as a reliable predictor of future streamflow in nival river basins across North America (Section 3)? In the discussion of our findings, we extract essential insights relevant to snow monitoring experts, forecasters, decision-makers, and workflow developers, addressing an important  
75 research gap in knowledge translation (Section 4).

## 2 Data and methods

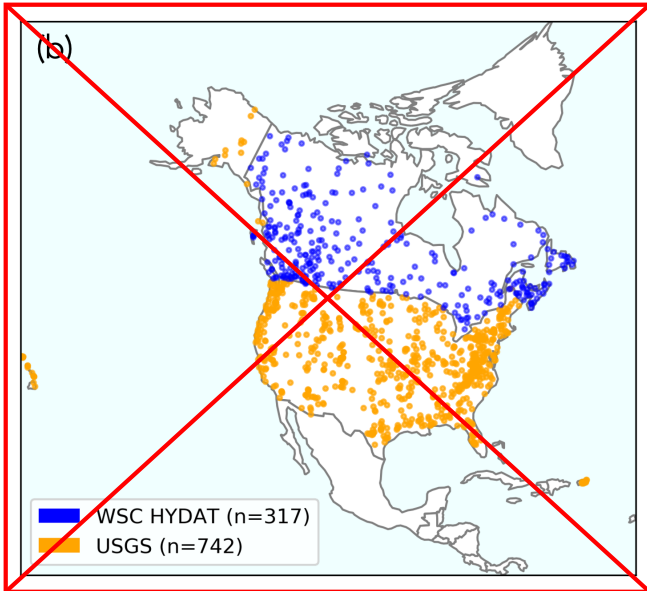
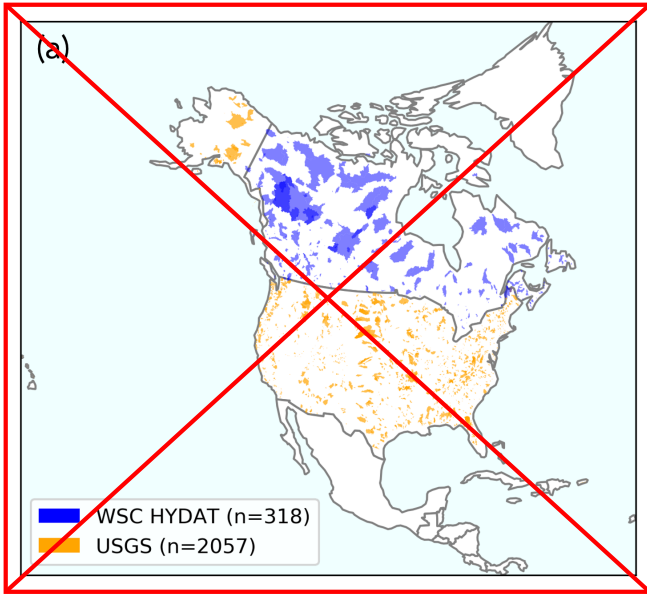
### 2.1 Data

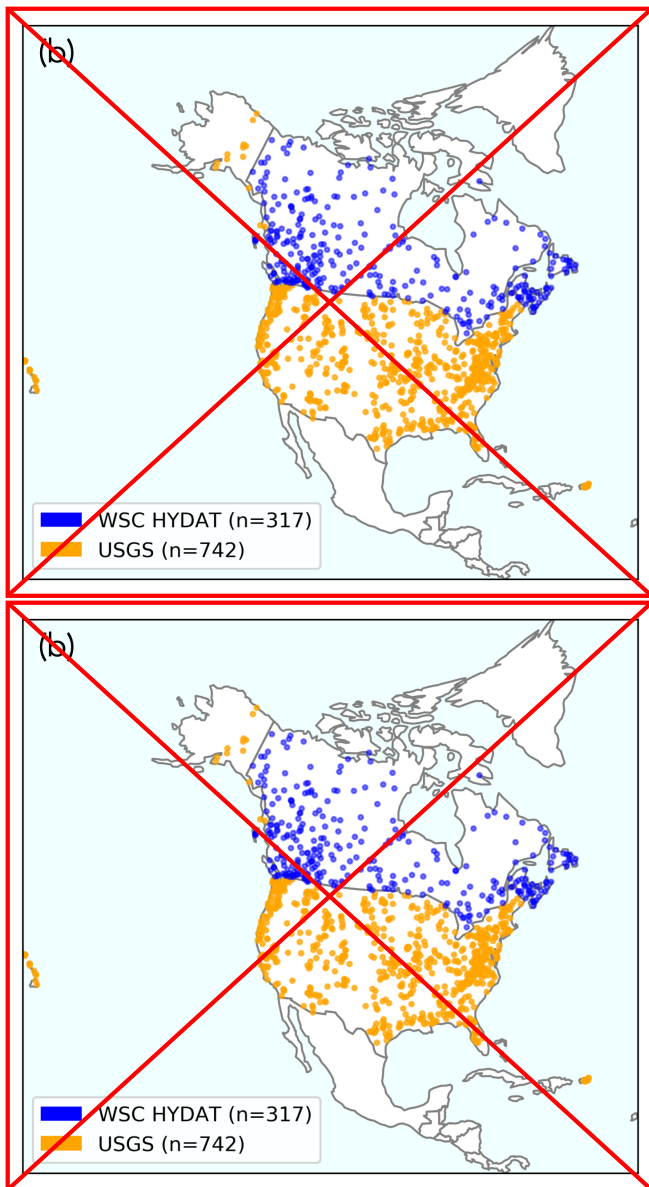
Four types of data are needed to run the workflow for North American river basins. These include river basin shapefiles and station data for streamflow, SWE and precipitation (Fig. 1). Each data type is explained in the following sections.



**Figure 1.** Maps of (a) basin outlines (a) and input station data - i.e., (b) streamflow (b), (c) SWE (c), and (d) precipitation (d) - across North America. Note that there are fewer streamflow stations than basin outlines as map (b) only shows streamflow stations with data for the period 1979–2021. Basin outlines and input station data discarded and not used for the analysis presented in this paper are shown in grey (see the basins selection process in Section 2.2.1). Note that the maps are zoomed in on the retained elements and some discarded basin outlines and stations may fall outside the map boundaries. Additionally, map (d) shows all SCDNA stations available. This includes stations with temperature data but no precipitation data, that were not used in this study.

80





### 2.1.1 Basin shapefiles and streamflow data

85 For the USA, we use shapefiles and streamflow observations for basins with limited regulation from the USGS Hydro-Climatic Data Network 2009 (HCDN-2009; Lins, 2012; Falcone, 2011). **HCDN-2009 comprises stations with minimal hydrological disturbance, measured by the presence of dams, freshwater withdrawal, including from groundwater, flow diversion, roads and other impervious surface areas, and pollutant discharges. Moreover, inclusion in the dataset necessitated a minimum of 20 years of continuous availability of streamflow data.**

90 For Canada, we use shapefiles and streamflow observations for basins with limited regulation from the Water Survey of  
Canada (WSC) HYDAT Reference Hydrometric Basin Network (RHBN) subset, called RHBN-N (ECCC, 2021). **The selection  
criteria for the HCDN-2009 and RHBN datasets exhibit substantial similarity, albeit with potential methodological nuances that  
may stem from varying priorities and contexts.** The reference hydrologic networks include only stations considered to have  
~~good quality data and were screened to avoid the influences of regulation, diversions, or land use change~~ **minimal or stable**  
95 **human impacts as defined by the presence of agricultural and urban areas, roads and a high population density, and the presence  
of significant flow structures (Whitfield et al., 2012).** RHBN-N was created to provide a nationally balanced network suitable  
for national studies. **Similarly to the HCDN-2009 dataset, a minimum data availability of 20 years of almost continuous  
streamflow records was required for a station to qualify.**

We downloaded streamflow data for the period 1979-01-01 to 2021-12-31 as data for this period were available for many  
100 stations in the dataset, and this was deemed an appropriate time series length for the purpose of this study. Data for the  
USA were downloaded from the National Water Information System (NWIS; USGS) using the Python package dataretrieval  
(Hodson and Hariharan, 2023). Data for Canada were downloaded from the WSC HYDAT database (ECCC, 2018) using the  
EASYMORE Python package (Gharari et al., 2023). See Fig. 1-(a) and (b) for maps of the basin shapefiles and streamflow  
stations that were retained.

### 105 **2.1.2 Snow Water Equivalent data**

Snow Water Equivalent (SWE) measurements were downloaded for the period 1979-10-01 to 2022-07-31. For Canada, mea-  
surements are from the Canadian historical Snow Water Equivalent dataset (CanSWE, Version V5; Vionnet et al., 2021b),  
available on Zenodo (Vionnet et al., 2023). CanSWE is a database of SWE data collected from numerous provincial/territorial,  
academic, and other agencies across Canada. Other measurements are from the Ministère de l'Environnement, de la Lutte  
110 contre les changements climatiques, de la Faune et des Parcs (MELCCFP) in Québec (Canada) and cannot be shared pub-  
licly. For the **western USA and Alaska**, measurements are mainly from the Natural Resources Conservation Service (NRCS)  
manual snow surveys and SNOTEL automatic snow pillows. The NRCS snow courses can be downloaded using the fol-  
lowing GitHub repository: <https://github.com/CH-Earth/snowcourse>. For the SNOTEL, we use data from the bias-corrected  
and quality-controlled (BCQC) dataset from the Pacific Northwest National Laboratory (PNNL; [https://www.pnnl.gov/data-](https://www.pnnl.gov/data-products)  
115 [products](https://www.pnnl.gov/data-products); Sun et al., 2019; Yan et al., 2018). **In the north-eastern USA, manual snow survey data were obtained from local  
agencies in the states of Maine, New Hampshire, New York, and Vermont. All the snow survey data collected in the USA and  
used in this study are available in the SWE dataset of Mortimer and Vionnet (2024).** Figure 1-(c) shows a map of the SWE  
stations used for this analysis. Note that snow data are missing in the northern central part of the USA, and a viable substitute  
in the future could be utilizing airborne gamma snow data (Cho et al., 2020), **as done by Mortimer et al. (2024) when validating**  
120 **gridded SWE products over North America.**

All SWE data used for this study were quality controlled (QC). In addition to the quality standards applied by the different  
data providers, a systematic QC procedure is described in Vionnet et al. (2021b) and was applied to all the snow data used in  
this study, with the exception of the already bias-corrected and quality-controlled SNOTEL dataset.

125 Several SWE stations appear to be overlapping in Fig. 1c. In various Canadian provinces and territories like Alberta, British Columbia, and the Yukon, automated snow stations and manual snow surveys are collected at the same sites. While the measurements from these stations generally agree, they are not identical due to micro-scale spatial variability. In addition, the stations overlap may partly be due to the scale of the map which does not allow to accurately display the variability of the snow measurements network in terms of position and elevation.

130 We use all available streamflow and SWE data and do not filter out data values based on their quality flags. The reason is that we perform gap filling of all time series within the workflow, and we trust that data providers are the most competent individuals to handle the initial infilling. We invite readers to refer to these datasets for a list of quality flags.

### 2.1.3 Precipitation data

Precipitation station data were downloaded from the Serially Complete Dataset for North America (SCDNA, Version 1.1) for the period 1979-01-01 to 2018-12-31 (Tang et al., 2020a). The SCDNA dataset is available on Zenodo (Tang et al., 2020b).  
135 Figure 1-(d) shows a map of the SCDNA stations.

## 2.2 Methods: Workflow

The workflow developed is structured in five Jupyter Notebooks: 1) Regime classification, 2) Streamflow pre-processing, 3) SWE pre-processing, 4) Forecasting, and 5) Hindcast verification. Each Notebook is coded in Python, and provides concise descriptions of its purpose, decisions, and underlying assumptions, whenever necessary, as well as a step-by-step overview  
140 of the annotated code, accompanied by visuals. The workflow, called FROSTBYTE (Forecasting River Outlooks from Snow Timeseries: Building Yearly Targeted Ensembles), is available on GitHub (Arnal et al., 2023a, v0.9.0). Note that the data downloading step (see Section 2.1) was not included in the GitHub workflow. Instead, sample data are provided for the Bow River at Banff (Alberta, Canada) and for the Crystal River ~~Abv~~Above Avalanche ~~Crk~~Creek, Near Redstone (Colorado, USA). Figure 2 provides a visual of the methods for each Jupyter Notebook. These will be described in more details in the sections  
145 below.



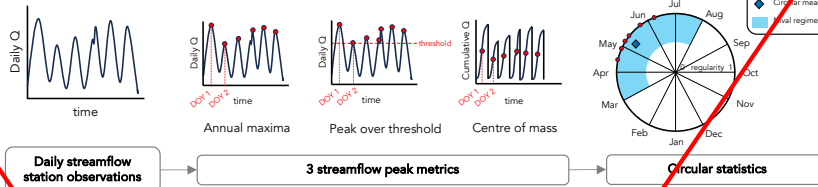


Figure 2. Detailed graphical methods for each Jupyter Notebook of the FROSTBYTE workflow.

### 1. Regime classification

[FROSTBYTE/notebooks/1\\_RegimeClassification.ipynb](#)

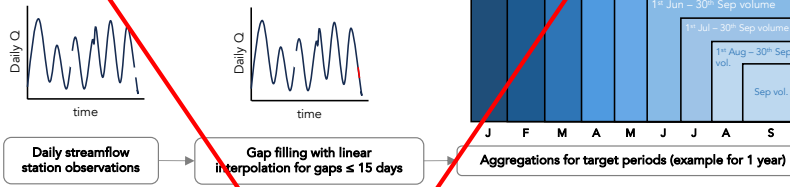
Circular statistics are computed on daily streamflow station observations to identify nival basins. We then sub-select nival basins with at least 20 years of overlapping SWE – Q data.



### 2. Streamflow pre-processing

[FROSTBYTE/notebooks/2\\_StreamflowPreprocessing.ipynb](#)

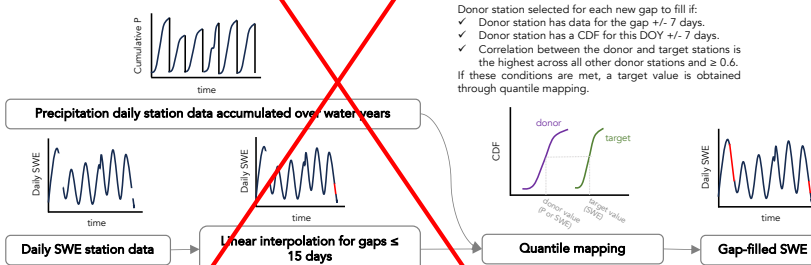
Daily streamflow timeseries are aggregated to seasonal volumes.



### 3. SWE pre-processing

[FROSTBYTE/notebooks/3\\_SWEPreprocessing.ipynb](#)

SWE station timeseries are gap filled using a combination of linear interpolation and quantile mapping from neighbour SWE and P stations.



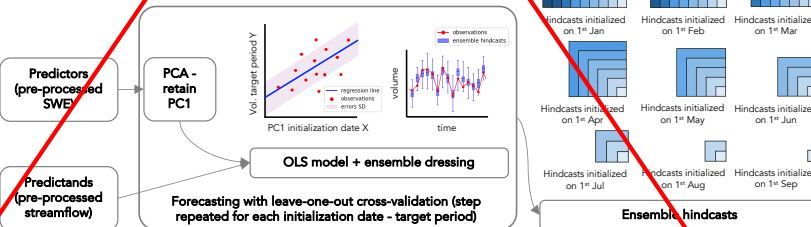
Donor station selected for each new gap to fill if:

- ✓ Donor station has data for the gap +/- 7 days.
  - ✓ Donor station has a CDF for this DOY +/- 7 days.
  - ✓ Correlation between the donor and target stations is the highest across all other donor stations and  $\geq 0.6$ .
- If these conditions are met, a target value is obtained through quantile mapping.

### 4. Forecasting

[FROSTBYTE/notebooks/4\\_Forecasting.ipynb](#)

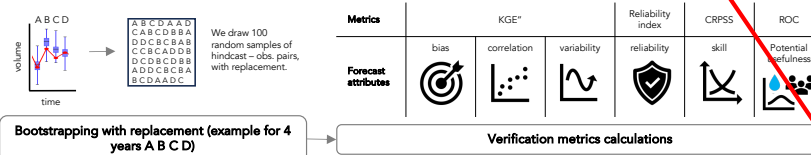
New ensemble volume hindcasts are generated on the 1<sup>st</sup> of each month between Jan. and Sep. using Principal Component Regressions.



### 5. Hindcast verification

[FROSTBYTE/notebooks/5\\_HindcastVerification.ipynb](#)

Deterministic and probabilistic verification metrics are computed to measure various aspects of the forecast quality, with bootstrapping.



### 2.2.1 Regime classification: Basins selection

To ensure the feasibility of producing forecasts using PCR from SWE predictors, we impose the following requirements on the basins used in this study:

- 150 – The basin must have a nival regime. Discussed in more detail in this section.
- The basin must contain at least one SWE station.
- The basin must have at least 20 years of overlapping SWE and streamflow data (**partially incomplete years are allowed** ~~regardless of whether the years are complete~~ as the data are further pre-processed to fill gaps, see Sections 2.2.2 and 2.2.3). If the basin contains multiple SWE stations, only one station needs to fulfill this requirement.

155 The river basins in the USA and Canada for which we collected data in the previous step (see Section 2.1) are subject to a wide range of hydroclimatic conditions. In this step, we ~~further~~ subset these basins to only keep basins that experience nival regimes - i.e., basins for which we can reasonably expect SWE to hold substantial predictability for streamflow forecasting. The existence of nival regimes can be inferred from climate classification schemes that account for the fraction of precipitation falling as snow in a given place. However, we instead opt to use an approach that identifies the typical flow regime for each  
160 basin based directly on the observed streamflow in that basin.

To classify the streamflow regimes, we used circular statistics (Burn et al., 2010). Circular statistics measure the timing and regularity of hydrological events such as flow peaks. For this study, three different streamflow peak metrics were used to provide more robust results than using a single metric, because strengths of one metric can compensate for weaknesses in another. Some of these weaknesses are discussed in Court (1962), Whitfield (2013), and Burn and Whitfield (2017).

165 The metrics used to identify peak flow events are [a] the streamflow annual maxima, [b] the streamflow peaks over threshold, and [c] the streamflow centre of mass (i.e., date on which 50% of the water-year streamflow occurs; Court, 1962); **see Fig. 2**. For the peak over threshold metric [b], the threshold was defined as the smallest annual maximum streamflow observed during the historical period in each basin. All metrics were computed using a water year from October 1<sup>st</sup> to September 30<sup>th</sup> of the following calendar year to link winter snow accumulation to the current year snowmelt. In order to maximize the amount of  
170 available data, we first performed gap filling through linear interpolation of the daily streamflow data. More information about the interpolation can be found in Section 2.2.2. Note that the streamflow interpolation was performed twice independently, once prior to the regime classification and once as part of the streamflow pre-processing, for a more logical flow of the workflow. The streamflow annual maxima [a] and the center of mass [c] metrics required complete years of data (i.e., any water year with missing observations was discarded), while the peak over threshold metric [b] allowed for incomplete years of data to identify  
175 peak flow events.

For each metric, we then calculated the average date of occurrence for these peak flow events by determining the circular mean of all event dates (**see Fig. 2**). Additionally, we assessed the regularity of the peaks by calculating the spread in the dates of occurrence of these events. The regularity value, which ranges between zero and one, provides a measure of how consistent the event dates are. Larger values indicate a higher level of regularity in the dates. Equations used for the regime classification

180 can be found in the Appendix. For each metric, we identified nival basins as those with an average date of occurrence of peak flow events between March 1<sup>st</sup> and August 1<sup>st</sup> and a regularity above or equal to 0.65 (defined based on results presented in Burn and Whitfield, 2023). We finally selected all nival basins identified by the three individual metrics.

185 **The streamflow linear interpolation could have impacted the regime classification, leading to missed flow peaks, especially for smaller river basins with faster response times. Nevertheless, all stations had nearly complete datasets, as this was a requirement for selection in the creation of both datasets (see Section 2.1.1). Furthermore, the use of three metrics for peak flow event identification, coupled with the utilization of the circular statistics method with a regularity threshold of 0.65, potentially mitigate some of these issues.**

## 2.2.2 Streamflow pre-processing

We processed the daily streamflow data for all previously identified nival basins (see Section 2.2.1) and converted them into 190 volumes that capture the spring freshet and that may be of interest of water users (e.g., for water supply management, hydropower generation, irrigation scheduling, early warnings of floods and droughts). These volumes serve as the predictands for the forecasting process (see Section 2.2.4).

We first performed gap filling through linear interpolation of the daily streamflow data in order to maximize the amount of available data. The maximum allowable gap length for interpolation was set to 15 days, consistent with the SWE interpolation 195 approach (see Section 2.2.3). **Due to the data availability quality checks conducted during the production of the HCDN-2009 and RHBN streamflow datasets, a one-step gap filling process was considered sufficient for streamflow, in contrast to the two-step gap filling performed for SWE (see Section 2.2.3).**

We then computed volumes for periods without any missing data for each nival basin: January 1<sup>st</sup> to September 30<sup>th</sup>, February 1<sup>st</sup> to September 30<sup>th</sup>, March 1<sup>st</sup> to September 30<sup>th</sup>, etc., until September 1<sup>st</sup> to 30<sup>th</sup> (see Fig. 2). Volumes are 200 calculated by summing the daily streamflow observations over the time periods mentioned above. These volume aggregation periods will be referred to as 'target periods' in the context of forecasting throughout this paper. The volumes dataset was saved for all basins as a NetCDF file.

## 2.2.3 SWE pre-processing

For each previously identified nival basin (see Section 2.2.1), we processed the SWE data to fill gaps **asbecause** the subsequent 205 Principal Component Analysis (PCA) does not allow ~~for~~ missing values. These pre-processed SWE data serve as the predictors for the forecasting process (see Section 2.2.4).

We selected SWE and precipitation (if any) stations located in each nival basin. The precipitation data is used to maximize the amount of data available as predictors. It was accumulated over water years for each precipitation station to serve as a proxy for SWE. To further enhance the availability of data, we applied linear interpolation to fill gaps in the daily SWE records. The 210 maximum allowable gap length for interpolation was set to 15 days, which aligns with the streamflow interpolation approach described in Section 2.2.2 and with the window of +/- 7 days used in the subsequent steps.

After applying linear interpolation, we then utilize quantile mapping to fill the remaining gaps using data from neighbouring stations (see Fig. 2). Subsequently, statistics necessary for the next gap filling steps quantile mapping were calculated for all extracted SWE and precipitation stations. Namely, a cumulative distribution function (CDF) was constructed for each station and for each day of the year (+/- 7 days). A CDF could only be constructed when at least ten data points were available. Spearman's rank correlation coefficients were calculated between each basin's SWE and precipitation station for each day of the year (+/- 7 days). Correlations could only be calculated when a minimum of three data points were available. It is important to note that the minimum sample size criteria for the CDF and the correlation calculations are user-defined. For this study, they were set to the values mentioned above in order to balance the need for a sufficiently large sample size for reliable results with the goal of filling in as many gaps as possible. The impact of these decisions could be explored in future research.

We then perform gap filling using quantile mapping by looping over SWE stations. For each missing SWE data point in a target station (i.e., the station requiring gap filling), a suitable SWE/precipitation donor station (i.e., the station providing data for infilling the target station's gap) was identified based on the following criteria:

- The donor station must have data on or around the date to be filled (within a window of +/- 7 days).
- The target and the donor stations should have a constructed CDF for the day of the year corresponding to the date to fill.
- The correlation between the target station and the donor station should be the highest amongst all potential donor stations and exceed a minimum correlation threshold of 0.6. Stations with correlations larger than but close to 0.5 could be deemed as only marginally correlated. We require a strong positive correlation to ensure the quality of the gap filling process and set the threshold to 0.6 for a station to be accepted as a donor station.

Based on these criteria, the value from the donor station closest to the date requiring filling is used to estimate the target station's value on the missing value's date. Note that the automatic SWE stations have a higher temporal frequency than the manual snow surveys, which could make the automatic stations preferable as potential donor stations.

As a result, a new gap-filled SWE dataset was generated and saved for each nival basin as a NetCDF file. Estimated values were clearly distinguished from the original observations using a specific flag.

Additionally, we developed an artificial gap filling function to enable users to assess the quality of the gap filling process. Results are shown for the Bow River at Banff (Alberta, Canada), one of the workflow testbeds, in the Appendix (Fig. A1 and A2). We do not show results for all other river basins as the artificial gap filling is not the primary focus of this study.

It is important to note that no threshold was set to define a total maximum allowable gap length for each station. Consequently, certain stations may have undergone substantial gap filling, as can be seen in Fig. A2. However, we speculate that setting such a threshold would have been counterproductive, as it would have significantly decreased the number of SWE stations available as predictors, thereby affecting the quality of the hindcasts produced. Additionally, linear interpolation might have impacted the construction of CDFs for donor and target stations, possibly introducing inaccuracies into the gap-filled data. Nevertheless, we speculate that utilizing a station's own data for gap filling via temporal interpolation could yield superior results compared to utilizing data from other stations, especially given the relatively gradual temporal variations in SWE.

## 2.2.4 Forecasting

Using the pre-processed predictors and predictands (see Sections 2.2.2 and 2.2.3) as inputs to an Ordinary Least Squares (OLS) regression model, we generate time series of ensemble hindcasts for each nival basin. Hindcasts are initialized on the first day of each month between January 1<sup>st</sup> and September 1<sup>st</sup> (both ends included) for target periods January 1<sup>st</sup> to September 30<sup>th</sup>,  
250 February 1<sup>st</sup> to September 30<sup>th</sup>, March 1<sup>st</sup> to September 30<sup>th</sup>, etc., until September 1<sup>st</sup> to 30<sup>th</sup>. See Fig. 2 for a graphical overview of the steps described below.

For each initialization date-target period combination, we first remove all years that have any missing values in the predictand and/or predictor datasets. We use a leave-one-out cross-validation approach for forecasting, whereby each data point in the dataset is sequentially withheld as a validation set, while the model is trained on the remaining data points. We require a  
255 minimum of eleven years of overlapping data in total, comprising ten years for training the regression model and an additional year for generating the hindcast, ~~using the leave-one-out cross-validation approach~~. Consequently, we may not be able to generate hindcasts for specific nival basins previously identified in Section 2.2.1, and for specific initialization date-target period combinations.

We then transform the gap-filled SWE from Section 2.2.3 into principal components (PC) to eliminate any intercorrelation  
260 amongst the SWE stations (Garen, David C., 1992). Principal Component Analysis (PCA) is a statistical method used to transform a set of intercorrelated variables into an equal number of uncorrelated variables. This step becomes particularly essential after gap filling, which might have introduced additional correlation among the SWE stations. In addition, the PCA is central to characterizing the spatio-temporal variability of the predictor variable. The first PC (i.e., the PC which captures most of the total variance in the set of variables) serves as the predictor for the forecasting process. In our analysis, the first PC  
265 explains 90% of the total variance in the gap filled SWE stations dataset, on average across all hindcast initialization dates and river basins. The explained variance of each principal component can be found in the Appendix (Fig. A3). We only select the first principal component in order to avoid any overfitting that could be caused by having too many predictors and a short time series. In a subseasonal climate forecasting study, Baker et al. (2020) showed that even using only the first two PCs could lead to overfitting for many river basins of the contiguous USA. We acknowledge however that this is a topic that warrants further  
270 exploration and discuss this in more detail in Section 4.4. We conduct a PCA and fit a new model for each predictor-predictand combination.

We subsequently split the predictor-predictand data using a leave-one-out cross-validation approach. We fit an Ordinary Least Squares (OLS) regression model on all years available for training. We then apply this model to the predictor year that was excluded, resulting in a deterministic volume hindcast for the corresponding target period. An ensemble of 100 members is then  
275 generated from this deterministic hindcast by drawing random samples from a normal (Gaussian) distribution. The distribution has a mean of zero and a standard deviation equal to the root mean squared error (RMSE) between the deterministic hindcasts and observations during the training period. We repeat this step until ensemble hindcasts have been generated for all years in the predictor-predictand dataset. It is important to note that hindcasts were generated only if there were at least ten years of overlapping predictand-predictor training data for a given initialization date-target period combination.

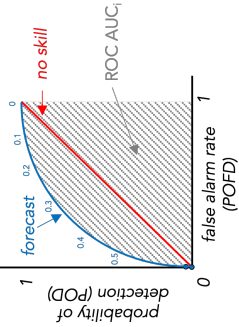
280 An independent regression model is used to produce an ensemble hindcast for each river basin, initialization date, target  
period, and year left out. Once we have generated hindcast time series for all initialization date-target period combination and  
all nival basins (when possible), each basin's hindcasts are individually saved in a new NetCDF file.

### 2.2.5 Hindcast verification

285 An overview of the various deterministic and probabilistic metrics used to assess the quality of the hindcasts, and what they  
measure, is provided in Table 1. To quantify sampling uncertainty, all metrics are computed using bootstrapping (Clark et al.,  
2021b). We draw 100 random samples of hindcast-observation pairs, with replacement.

To enable a meaningful comparison of performance across different basins, we defined specific target periods that capture  
each basin's peak flow (Qmax). We refer to these periods as 'periods of interest' throughout the paper. For each nival basin, the  
period of interest begins in the month of the basin's Qmax and extends until the end of the water year. For example, if a basin  
290 has its Qmax on May 15<sup>th</sup>, its period of interest will be May 1<sup>st</sup> to September 30<sup>th</sup>.

**Table 1.** Overview of the various deterministic and probabilistic metrics used to assess the quality of the hindcasts.

Metric	Description	Equation
<b>KGE"</b>	The Kling-Gupta Efficiency (KGE) is a deterministic and combined measure of the forecast correlation, bias and variability (Gupta et al., 2009). The KGE" was proposed by Tang et al. (2021) to solve issues arising with <b>mean values close to 0 values</b> in the KGE or KGE'.	$KGE'' = 1 - \sqrt{\beta^2 + (\alpha - 1)^2} + (\rho - 1)^2$ <p>KGE" is unitless and ranges between <math>-\infty</math> and 1, with a perfect score of 1. This metric was computed on the ensemble hindcast medians. Equations for the components of the KGE" can be found in the Appendix.</p>
<b>RI</b>	The reliability index (RI) is a probabilistic measure of the forecast reliability - i.e., the adequacy of the forecast ensemble spread to represent the uncertainty in the observations. More specifically, it measures the average agreement between the predictive distribution and the observations by quantifying the closeness between the empirical CDF of the ensemble forecast with the CDF of a uniform distribution (Renard et al., 2010; Mendoza et al., 2017).	$RI = 1 - 2\alpha' = 1 - 2 \left[ \frac{1}{N} \sum_{i=1}^N  P_i(o_i) - U_i(o_i)  \right]$ <p>RI is unitless and ranges between 0 and 1, with a perfect score of 1. Note that <math>\alpha</math> is often used as a symbol for the reliability index. Here, we use the notation RI instead so as not to confuse this metric with the KGE" variability ratio (<math>\alpha</math>).</p>
<b>Fair CRPSS</b>	The Continuous Rank Probability Skill Score (CRPSS) is a probabilistic measure of the forecast skill - i.e., the performance (in terms of the CRPS) of the ensemble forecast against a baseline (here, the observed climatology). The CRPS is a measure of the difference between the predicted and the observed cumulative distribution functions (CDF) (Hersbach, 2000). <b>Here, we use a fair version of the CRPS to account for the different ensemble sizes of the forecast and the baseline (Ferro et al., 2008; Ferro, 2014; Zamo and Naveau, 2018).</b>	$FairCRPSS = 1 - \frac{FairCRPS_{forecast}}{FairCRPS_{baseline}}$ <p>where <math>CRPSS = \frac{1}{N} \sum_{i=1}^N \int_{-\infty}^{\infty} [F_i(q) - F_o(q)]^2 dq</math></p> $FairCRPSS = \frac{1}{M} \sum_{i=1}^M  x_i - y  - \hat{\lambda}_2$ <p><b>Fair</b> CRPSS is unitless and ranges between <math>-\infty</math> and 1, with a perfect score of 1. <b>Fair</b> CRPSS=0 represents the threshold below which hindcasts have no skill compared to the baseline.</p>
<b>ROC</b>	The Relative Operating Characteristic (ROC) is a probabilistic measure of the forecast resolution - i.e., the ability of the forecast to discriminate between events and non-events (Mason and Graham, 2002). Here, the ROC was computed for low/high flows (i.e., flows below/above the lower/upper tercile of the observed climatology). This metric can serve as an indicator of the forecast's 'potential usefulness' and is of particular importance for decision-makers (Arnal et al., 2018; Emerton et al., 2018).	 <p> <math>POD = \frac{hits}{hits + misses}</math>  <math>POFD = \frac{correct\ negatives + false\ alarms}{correct\ negatives + false\ alarms}</math> </p> <p>The ROC area under the curve (or ROC AUC) is unitless and ranges between 0 and 1, with a perfect score of 1. ROC AUC=0.5 represents the threshold below which hindcasts have no skill.</p>

$F_i(q)$ : ensemble forecast CDF;  $F_o(q)$ : observations CDF;  $P_i(o_i)$ : empirical CDF of the ensemble forecast p-values for year  $i$ ;  $U_i(o_i)$ : uniform distribution  $U[0,1]$ ;  $x_i$ : member  $i$  of ensemble forecast with size  $M$ ;  $y$ : corresponding observation;  $\hat{\lambda}_2$ : expectation of the CRPS, unbiased when the members are independently sampled from the forecast distribution (see Zamo and Naveau (2018)).



To guide the hindcasts' evaluation, we formulate two hypotheses regarding the hindcasts generated using this approach:

1. The hindcast performance is expected to be better for hindcasts initialized around the peak SWE in each basin.
2. Higher hindcast quality is anticipated for hindcasts with high antecedent SWE content and low precipitation during the hindcast target period in each basin.

295 To support the interpretation of the hindcast evaluation and verify those hypotheses, we computed two additional measures. To evaluate the first hypothesis, we calculated the 'SWE content' for all initialization dates (i.e., note that forecasts were initialized on the 1<sup>st</sup> of each month between January and September for computational reasons, and that we may as a result miss peak SWE). We calculated the median percentage of maximum SWE for each initialization date across all available years of data for all SWE stations. The maximum SWE value was determined for each water year for this calculation. E.g., A median  
300 percentage of maximum SWE of 50% indicates that across all years for which we have data for a given SWE station, in the median year, half of that year's maximum SWE is present at that location on the forecast initialization date. The equation to calculate the 'SWE content' can be found in the Appendix.

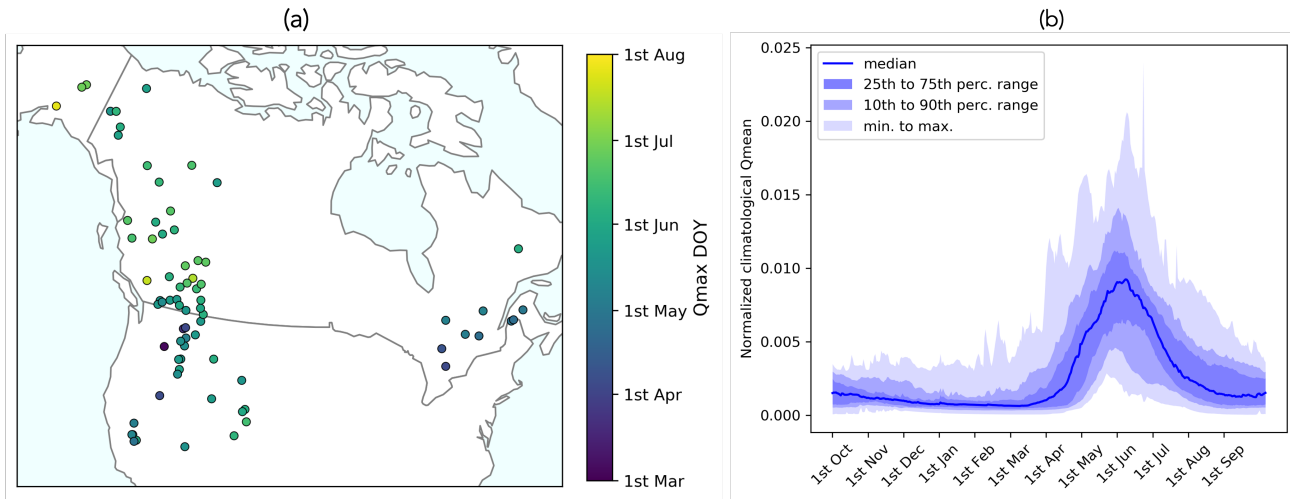
To evaluate the second hypothesis, we computed the ratio of precipitation to SWE (i.e., P/SWE). To achieve this, we followed these steps for each basin:

- 305
- We calculated the precipitation accumulation for each year, target period, and each precipitation station within the basin. We then calculated the climatological medians for precipitation accumulation, considering each station and target period, and subsequently averaged them over the entire basin. This gave us the basin-averaged precipitation accumulation climatological medians for each target period.
  - We calculated the SWE climatological median for each initialization date and each SWE station within the basin. We  
310 then averaged the SWE climatological medians over the entire basin, resulting in basin-averaged SWE climatological medians for each initialization date.
  - Finally, we divided the basin-averaged precipitation statistics by the corresponding basin-averaged SWE statistics for each combination of initialization date and target period.

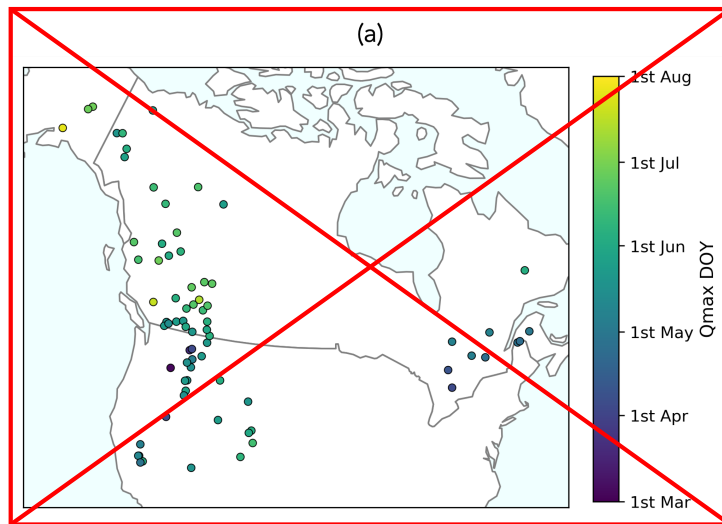
### 3 Hindcast evaluation

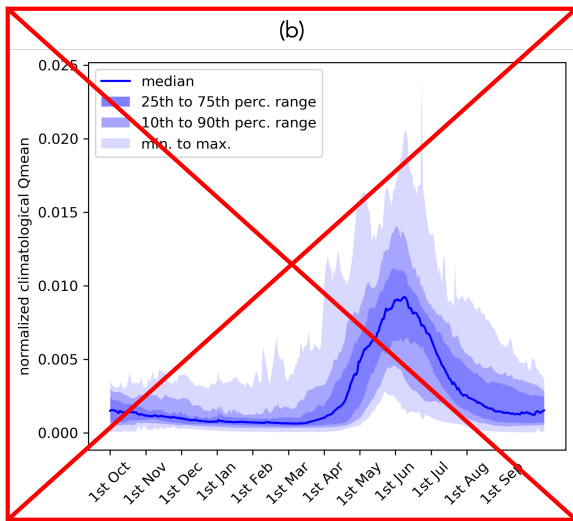
315 In this section, we quantify the range of predictability for 62 of the 75 identified nival basins across North America (Fig. 3) by analyzing results for various deterministic and probabilistic metrics, as outlined in Section 2.2.5. A total of 13 basins were excluded from this analysis as no hindcasts could be generated for those basins **given due to** a limited amount of overlapping predictor-predictand training data (as outlined in Section 2.2.4).

The figures presented in the sub-sections below display only the bootstrapping means. The corresponding bootstrapping  
320 ranges, showing the uncertainty in these estimates, can be found in the Appendix (Fig. A7).



**Figure 3.** Map and hydrographs of the 75 nival basins with limited regulation that meet the data requirements. Basins identified as having a nival regime that did not meet the data requirements are shown in the Appendix (Fig. A4). (a) The map shows the average day of the year (DOY) when the maximum streamflow ( $Q_{max}$ ) occurs for each nival basin. (b) The hydrographs displays the normalized climatological mean streamflow for all 75 nival basins (i.e., the daily fraction of total annual streamflow), with the median across all basins as the blue line and the variation in responses across all basins indicated by the shaded percentiles. ~~The climatological mean streamflow timeseries for each basin was normalized by dividing it by the sum of the timeseries.~~





### 3.1 Correlation, bias, and variability

Figure 4 shows the hindcast performance in terms of the Kling-Gupta Efficiency (KGE) and its decomposition into correlation, variability, and bias in the different subplots. In each subplot, results are shown for each hindcast target period (coloured lines), as a function of hindcast initialization dates (x-axis). Looking at the KGE for hindcasts produced for the target period September 1<sup>st</sup> to 30<sup>th</sup> (purple line) as an example, we observe the evolution in performance over time, from hindcasts initialized on 1<sup>st</sup> January (left-most dot) to those initialized on 1<sup>st</sup> September (right-most dot). The hindcasts' lead time decreases progressively from left to right within each subplot. The KGE can vary significantly across different target periods, and these differences tend to increase with later initialization dates. This highlights the impact of both target periods and model initialization on the hindcast quality. Overall, the KGE is higher for early target periods and decreases with later target periods. This hints that the snowpack holds less predictability as we move from the spring to the summer/fall months, and may be an indication of a shift from snow to rain as the dominant driver of streamflow.

For hindcasts generated for target periods January 1<sup>st</sup> to September 30<sup>th</sup> until June 1<sup>st</sup> to September 30<sup>th</sup>, the KGE increases towards the perfect value as we are approaching the start of the target period being predicted (i.e., with 0 lead months - e.g., hindcasts for June 1<sup>st</sup> to September 30<sup>th</sup> initialized on June 1<sup>st</sup>). Later target periods (August 1<sup>st</sup> to September 30<sup>th</sup> and September 1<sup>st</sup> to 30<sup>th</sup>) show a declining KGE overall. Hindcasts for July 1<sup>st</sup> to September 30<sup>th</sup> show a mixed signal: they follow the later target periods' curves but peak for the June 1<sup>st</sup> initialization, after which they quickly decline.

The correlation and the variability ratio show similar patterns to the KGE. The variability tends to be underestimated overall. This may be a direct consequence of using only PC1 as a predictor, although further comprehensive testing would be required to confirm this. The bias ratio is overall slightly positive, indicating that the hindcast medians overall overestimate the observed volumes. This is especially noticeable for hindcasts initialized between July 1<sup>st</sup> and September 1<sup>st</sup>.

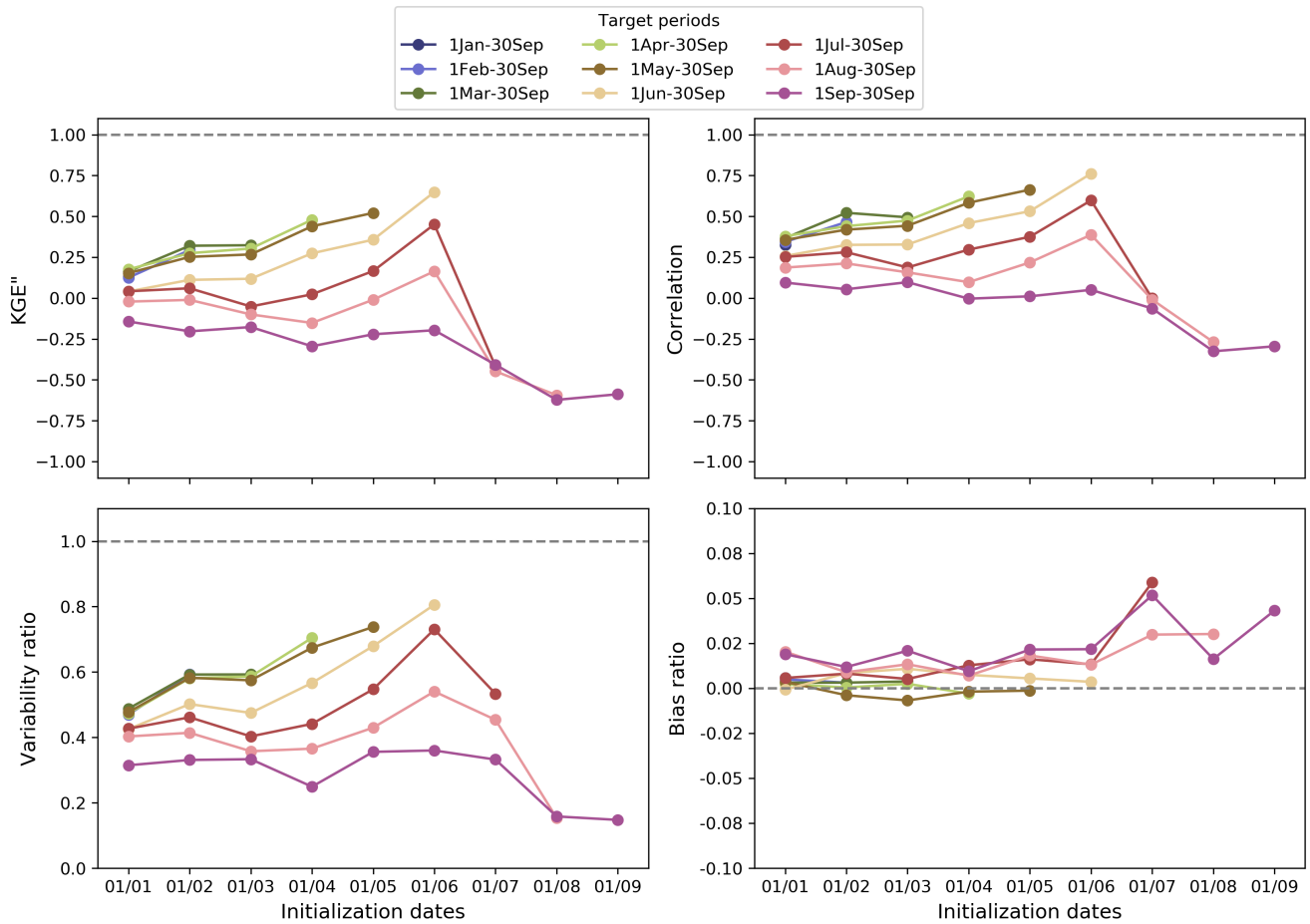


**Figure 4.** KGE" of the hindcast medians and its decomposition (i.e., correlation, variability, and bias) as a function of hindcast initialization dates. Each line displays median values across all basins for each target period. On all plots, the dashed lines represent the perfect value for each metric. Refer to Table 1 for the KGE" equation.

### 3.2 Reliability

Figure 5 shows the hindcast reliability, measured with the reliability index, as a function of hindcast initialization dates. From the literature, we expect the hindcasts generated to have high reliability given the ensemble generation approach used (i.e., statistical analysis of errors in cross-validated hindcasts, compared to other methods, such as using an ensemble of models or an ensemble of meteorological inputs without any pre-processing). Indeed, overall, hindcasts display a high reliability index (ranging between 0.55 and 0.9) across all river basins, initialization dates, and target periods.

The reliability of hindcasts is not entirely perfect, primarily due to the leave-one-out cross-validation approach used. We expect this effect to be more noticeable when the sample size is smaller, and hypothesize that it may partially account for the decrease in hindcast reliability with increasing initialization dates observed here.

The lower reliability for the September 1<sup>st</sup> to 30<sup>th</sup> target period additionally provides further support for the diminishing significance of snow information during periods characterized by non-snowmelt-driven flow.

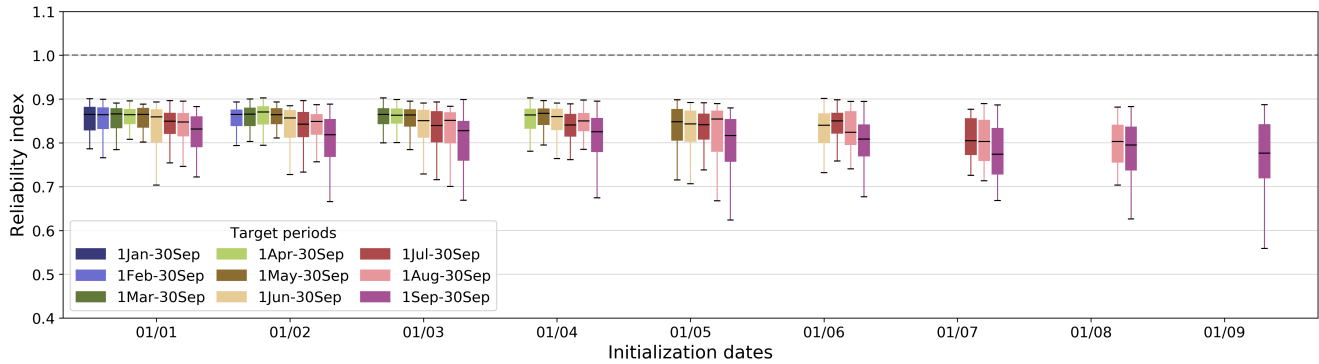
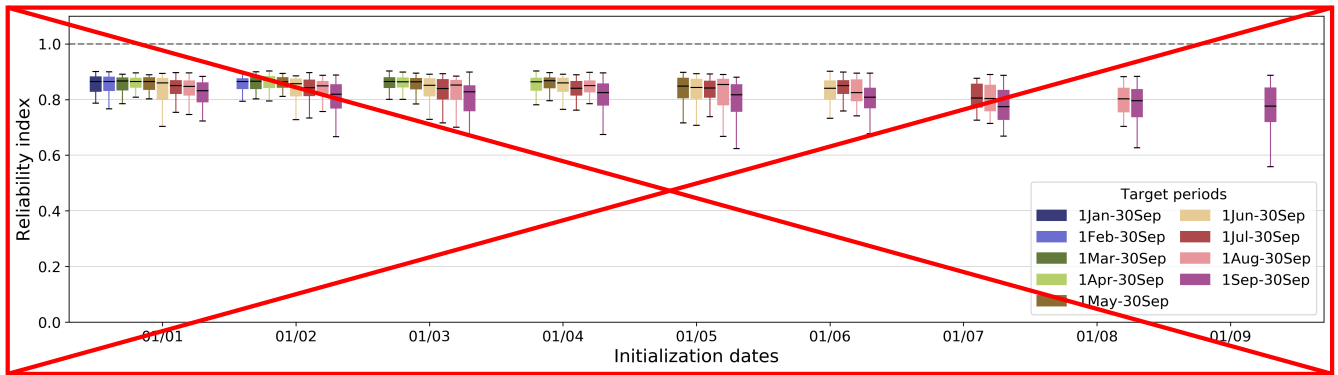


**Figure 5.** Hindcast reliability as a function of hindcast initialization dates. The boxplots display values for all basins. The dashed line represents the perfect value. Refer to Table 1 for the reliability index equation.



### 355 3.3 Skill

Figure 6 shows the hindcast skill in terms of the Fair Continuous Rank Probability Skill Score (Fair CRPSS), as a function of hindcast initialization dates. On average, hindcasts are as good as the baseline when they are initialized on January 1<sup>st</sup>. They gradually get more skilful (i.e., better than the observed streamflow climatology) for initialization dates between February 1<sup>st</sup> and June 1<sup>st</sup>. Beyond June 1<sup>st</sup>, hindcasts for the summer/fall target periods exhibit no overall skill (i.e., worse than the observed streamflow climatology). Overall, earlier target periods have better skill than the later target periods. This is similar to the pattern observed for the KGE" and again hints at a shift from snow to rain as the dominant driver of streamflow. It further suggests that as we approach peak SWE (see Fig. 9-(a) in Section 4.1), we can extract more valuable information and enhance the hindcast skill.

This SWE-based forecasting approach is unskilful with later initialization dates and target periods, meaning that using the streamflow climatology provides better results than using this approach. Note that the Fair CRPSS results might be impacted

by the ensemble size of the hindcasts (100 members) compared to the ensemble size of the baseline (the number of members equals the number of years in the climatology, excluding the year being forecasted, and varies across basins and target periods).

As shown by the boxplots' span, the Fair CRPSS can vary considerably across different basins. This implies that the predictive performance might differ significantly depending on the geographical location. To explore the geographical distribution of the Fair CRPSS, we show maps of the Fair CRPSS with zero to six months lead time (Fig. 7). Note that the lead months are different from the initialization dates of the hindcast, where lead month refers to the number of months between the hindcast initialization date and the target period start. The Fair CRPSS maps show results for each basin's period of interest only, in order to be able to compare results across river basins for a single lead time. Overall, the Fair CRPSS decreases with increasing lead time, and by at three to four or more months lead time the skill is on average marginal there is little skill evident. Note that some basins may show increasing skill with increasing lead time, or a more complex picture, highlighting the intricate interplay between initialization date and target period.

Results are very variable across space, and some river basins already show low to no or negative skill throughout all lead months, and the skill drops quickly after zero months lead time. These are mostly basins situated in the northwest and in the east. Pockets of higher skill are seen across several lead months for basins situated in western North America, in and around the Rocky Mountains and the Sierra Nevada mountain ranges. Figure A5 in the Appendix displays river basins which consistently exhibit negative skill, as well as those consistently demonstrating high skill. On the other hand, some basins display low to no skill throughout all initialization dates. We speculate that basins exhibiting higher skill are those characterized by substantial contributions of SWE to streamflow predictability and substantial year-to-year variability, thereby enhancing skill in comparison to the climatological reference.

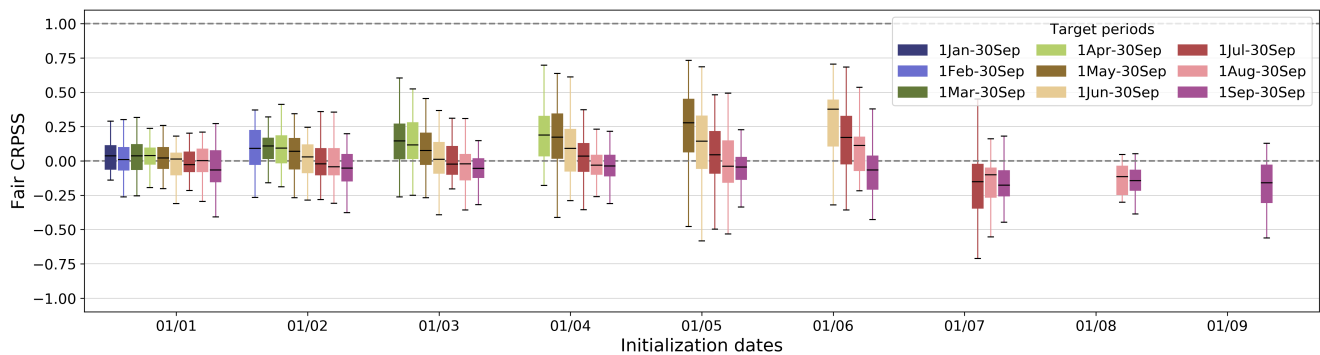


**Figure 6.** Hindcast Fair CRPSS for each target period as a function of hindcast initialization dates. The boxplots display values for all basins. The upper dashed line (Fair CRPSS=1) represents the perfect value and the lower dashed line (Fair CRPSS=0) represents the threshold below which hindcasts have no skill compared to streamflow climatology. Refer to Table 1 for the Fair CRPSS equation.

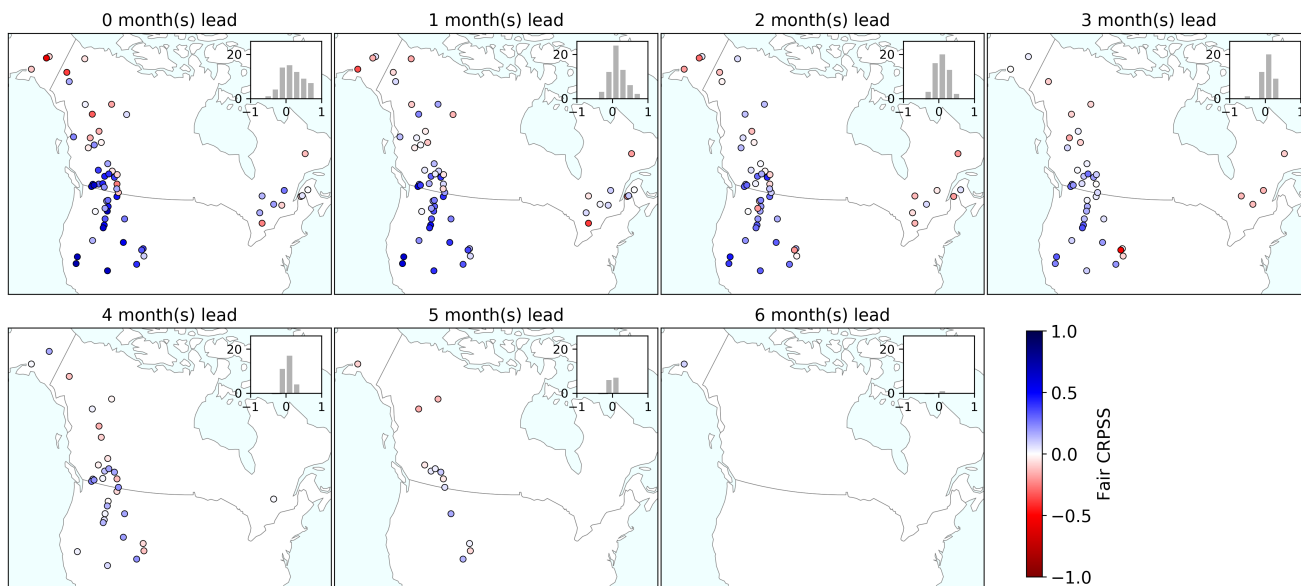
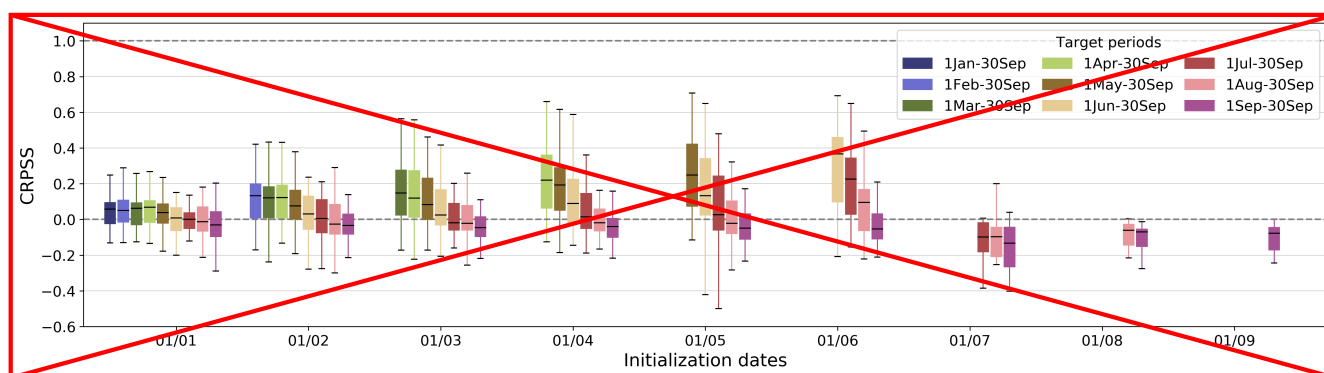
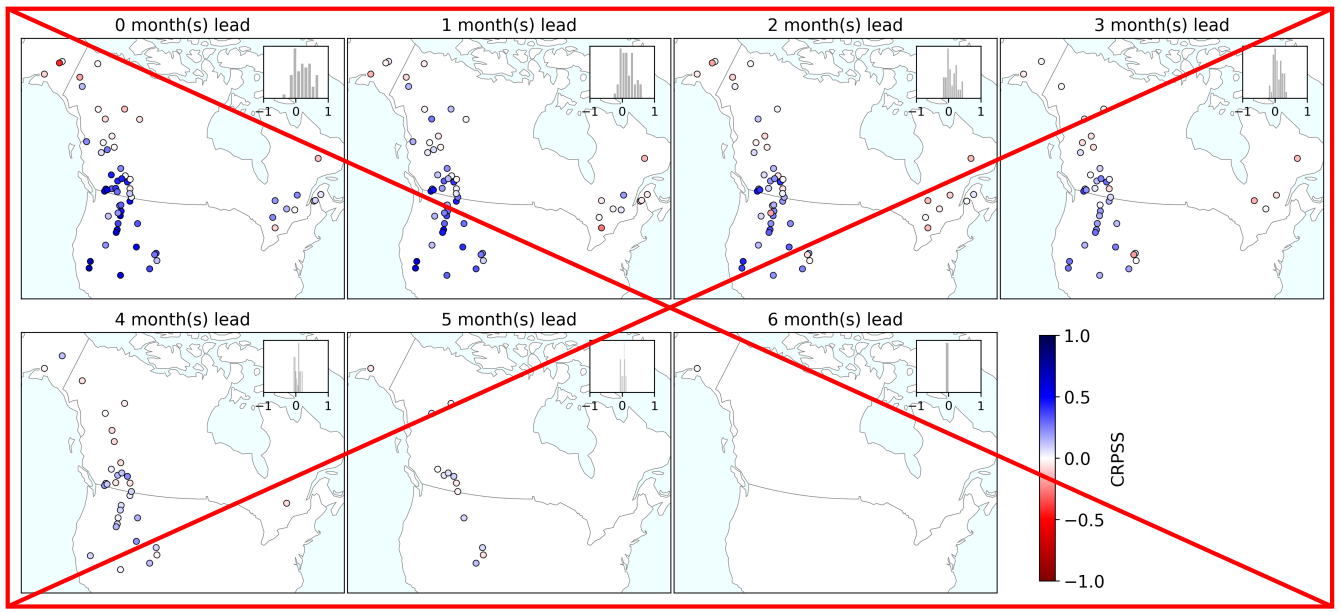


**Figure 7.** Maps of the hindcast Fair CRPSS for hindcasts from zero to six months lead time and inset histograms showing the distribution of Fair CRPSS values. Each subplot shows results for the target period of interest within each river basin. Note that initialization dates and periods of interest are not shown explicitly here. For instance, the first map, showing the Fair CRPSS for hindcasts with zero months lead time, will include results from hindcasts of January 1<sup>st</sup> to September 30<sup>th</sup> initialized on January 1<sup>st</sup>, as well as from hindcasts of February 1<sup>st</sup> to September 30<sup>th</sup> initialized on February 1<sup>st</sup>, etc. On the other hand, the last map, showing the Fair CRPSS for hindcasts with six months lead time, will include results from hindcasts of July 1<sup>st</sup> to September 30<sup>th</sup> or later, initialized on January 1<sup>st</sup> or later. The number of river basins shown on each map varies based on the lead time, reflecting the period of interest being forecasted (e.g., a river basin with a January 1<sup>st</sup> to September 30<sup>th</sup> period of interest cannot be forecasted with more than zero months lead time, after the 1<sup>st</sup> of January). The last subplot (i.e., six months lead time) shows results for a single river basin situated in Alaska.



385



### 3.4 Potential usefulness

Figure 8 shows the hindcast potential usefulness in terms of the Relative Operating Characteristic area under the curve (ROC AUC), as a function of hindcast initialization dates, for predicting (a) high flows and (b) low flows. Unlike plots for the KGE" and its decomposition, the reliability index, and for the Fair CRPSS (boxplots only), these plots show results for each basin's period of interest only, as we are interested in understanding the predictability of higher or lower than normal volumes during the basin's peak flow period. Results for low and high flows are very similar, which could be related to the high hindcast reliability, and will be described jointly below.

For all target periods/periods of interest, the ROC AUC increases with later initialization dates, reaching a peak with hindcasts generated on May 1<sup>st</sup>/June 1<sup>st</sup>. This suggests that the potential usefulness of these hindcasts increases as lead-time decreases. It is however not the case for hindcasts for July 1<sup>st</sup> to September 30<sup>th</sup>, where the ROC AUC decreases after June 1<sup>st</sup>. For most target periods of interest, peak ROC AUC is obtained for hindcasts with zero months lead time (higher ROC AUC is better). For example, the ROC AUC of hindcasts for May 1<sup>st</sup> to September 30<sup>th</sup> is the highest when the hindcasts are initialized on May 1<sup>st</sup>. The ROC AUC, and therefore the potential usefulness, of most hindcasts decreases with increasing lead time. This is however not the case for hindcasts for July 1<sup>st</sup> to September 30<sup>th</sup>, where the ROC AUC is highest when hindcasts are initialized on average on May 1<sup>st</sup> (with two months lead time). This hints again at a shift from snow to rain as the dominant driver of streamflow between the spring and the summer/fall months.

The hindcast potential usefulness varies for different target periods and the hindcasts generated for the target periods March 1<sup>st</sup> to September 30<sup>th</sup> and May 1<sup>st</sup> to September 30<sup>th</sup> show the best performances, indicating better predictions for low and high flows during these periods. Conversely, the hindcasts produced for the target periods April 1<sup>st</sup> to September 30<sup>th</sup>, June 1<sup>st</sup> to September 30<sup>th</sup>, and July 1<sup>st</sup> to September 30<sup>th</sup> exhibit the worst performances, implying less predictability for low and



high flows for these specific periods. Overall, for all periods of interest except for July 1<sup>st</sup> to September 30<sup>th</sup> there is potential usefulness in predicting low and high flows from January 1<sup>st</sup>.

As these plots show results for each basin's period of interest only, some of the boxplots have limited data points (e.g., the  
410 ~~boxplots for April 1<sup>st</sup> to September 30<sup>th</sup> are created from results for nine river basins only~~) (i.e., the number of data points in  
each boxplot is shown in Fig. 8c). This could explain some of the differences between boxplot span and the variability or noise  
observed in each subplot. Figure A6 in the Appendix shows results for individual basins.

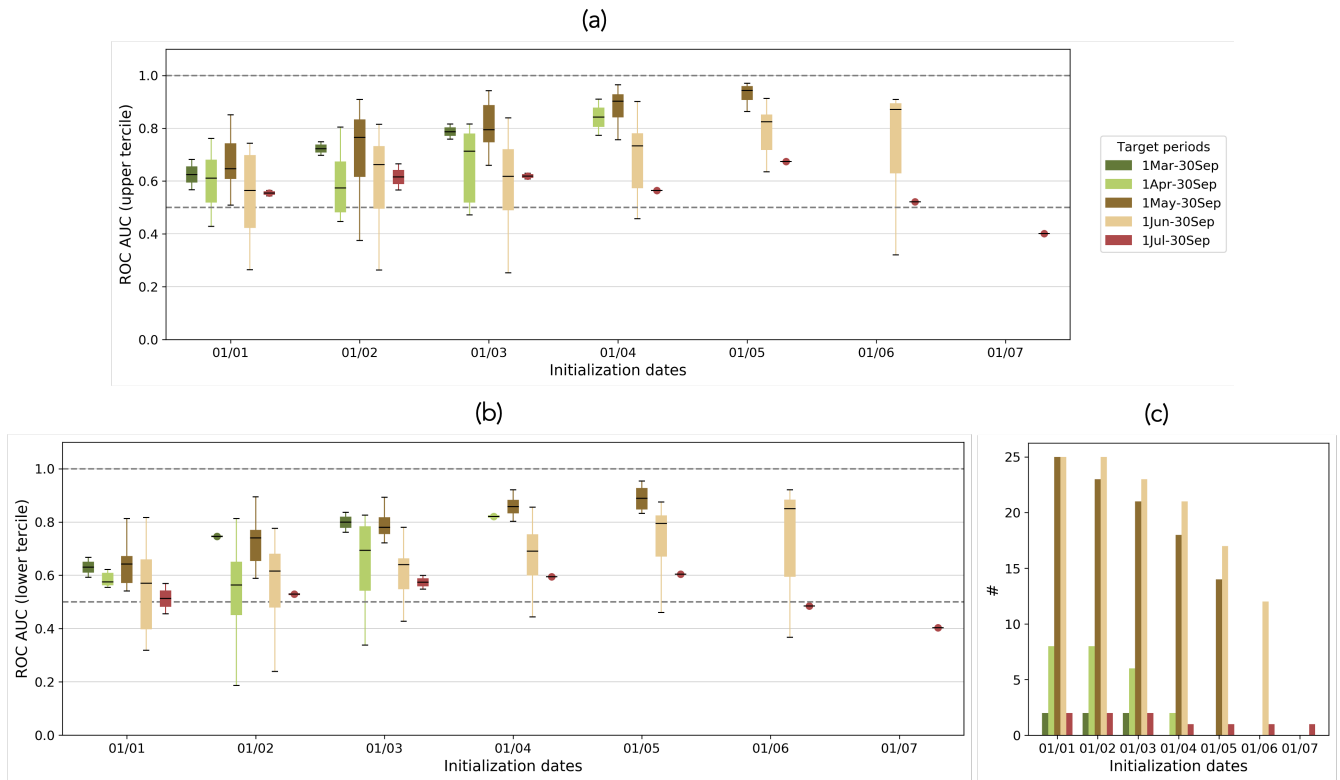
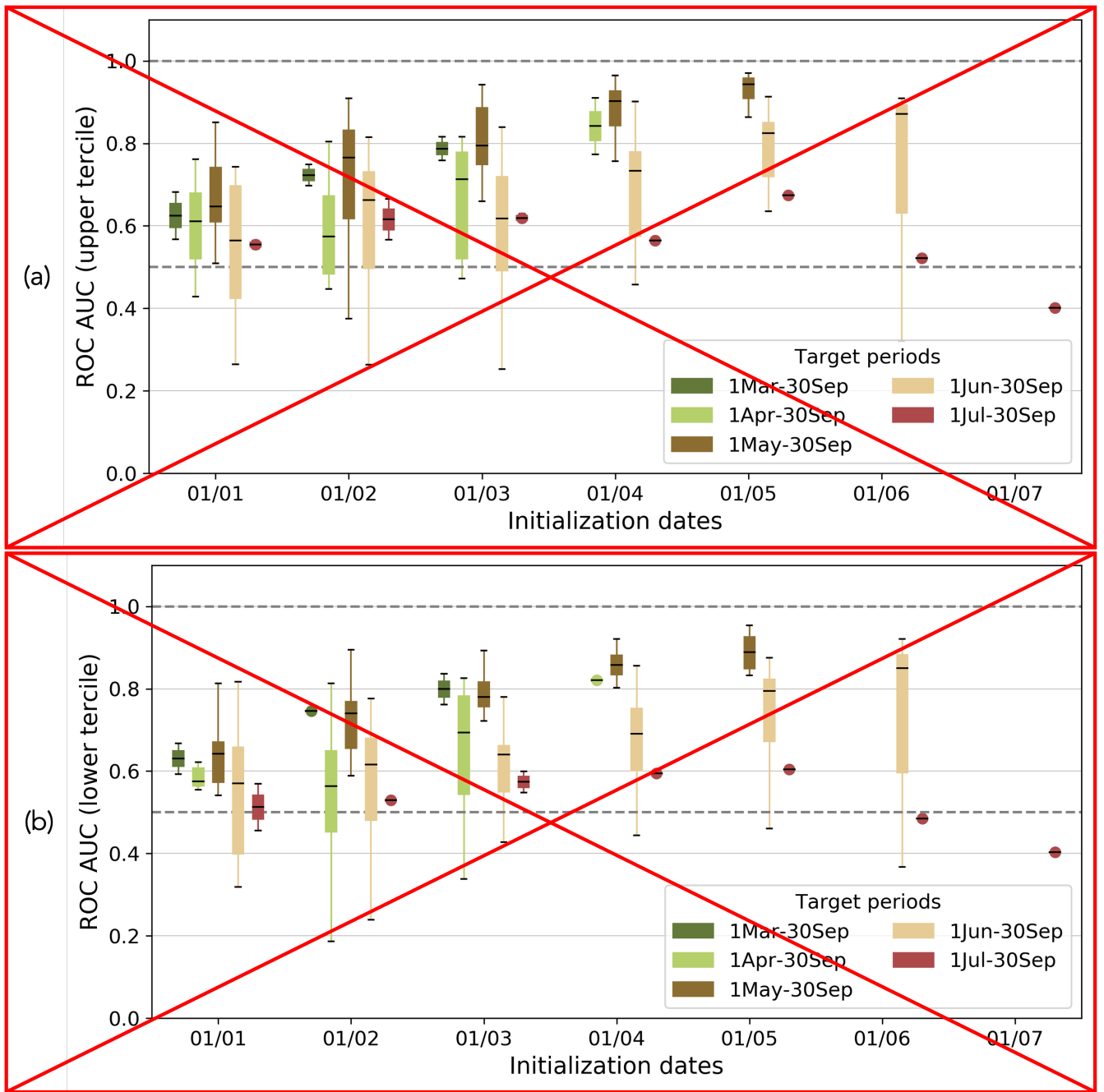


**Figure 8.** Hindcast ROC AUC for each target period as a function of hindcast initialization dates for (a) flows above the climatology upper tercile and (b) flows below the climatology lower tercile. The boxplots display values for all basins, where their period of interest coincides with one of the target periods. **The number of river basins in each boxplot is shown in panel (c).** The upper dashed line (ROC AUC=1) represents the perfect value and the lower dashed line (ROC AUC=0.5) represents the threshold below which hindcasts have no skill. **Refer to Table 1 for the ROC AUC calculation.**



#### 415 4 User-oriented discussion

We now draw insights relevant for snow monitoring experts, streamflow forecasters, decision-makers, and workflow developers from the results presented in Section 3.

## 4.1 Snow monitoring experts

For this discussion, snow monitoring experts include snow surveyors, field collection technicians, and monitoring network designers. Collectively, they conduct valuable work to support many different scientific and applied questions. An important use of snow surveys is water supply outlooks. As such, it is worth considering the following questions:

- Which SWE measurement dates are most important for forecasting streamflow volumes?
- Where and when are more SWE data needed for improving streamflow forecasts?

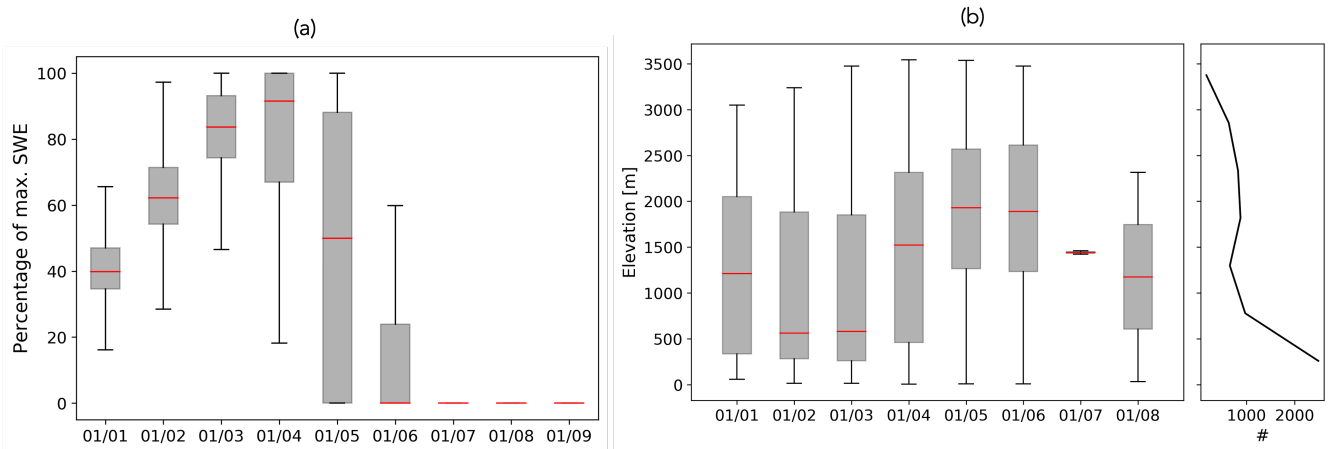
The first question relates to our **first** hypothesis that the highest performances can be found for hindcasts initialized around the peak SWE date in each basin (see Section 2.2.5). While peak SWE typically occurs around April 1<sup>st</sup> across North America (Fig. 9-(a)), the results presented in Section 3 reveal that high performance in streamflow forecasts can still be achieved by using SWE observations up until June 1<sup>st</sup>. This suggests that persistent snowpack (i.e., after April 1<sup>st</sup>) can hold important predictability for spring/summer streamflow volumes. Thus, the SWE measurement dates after peak SWE are critical for skilful predictions of streamflow.

The importance of SWE measurement dates depends on station elevation (and possibly also latitude; not shown). As seen with the boxplots in Fig. 9-(b), the timing of peak SWE exhibits a noticeable variation with station elevation, where, in general, stations situated at higher elevations have later peak SWE. On average, stations with peak SWE on February 1<sup>st</sup> and March 1<sup>st</sup> are at lower elevations than stations with peak SWE on April 1<sup>st</sup>, May 1<sup>st</sup>, and June 1<sup>st</sup>. It is evident in the accompanying line histogram in Fig. 9-(b) that the majority of SWE stations are concentrated at lower elevations. While snow depth and SWE generally increase with elevation, maximum snow depth in mountainous areas typically occurs near the tree line, with some variability across different sites due to variations in canopy cover (Cartwright et al., 2020; Grünewald et al., 2014). This suggests that SWE measurements at mid- to high-elevations best capture peak SWE in these basins.

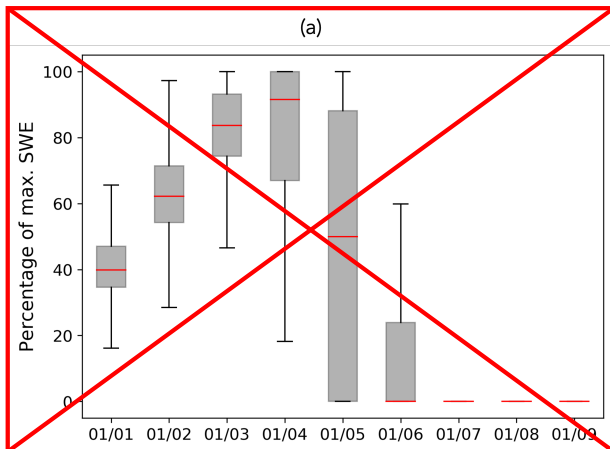
This brings us to the second question: where and when are more SWE data needed for improving streamflow forecasts? Given the importance of mid- to high-elevation SWE and the limited measurements at these elevations, measurement dates later in the snow season are necessary to capture the timing and magnitude of maximum SWE and the evolution of snowmelt to predict snowmelt-driven runoff. Investigating the use of snow pillows, snow scales, and snow depth sensors is recommended to provide continuous depth and SWE measurements at point-based survey sites, thus increasing SWE temporal coverage. Expanding spatial coverage of point-based surveys to include more mid- to high-elevation areas may pose challenges due to the difficulty of reaching these locations and the manual labour needed to set up and maintain such sites. This work can hopefully serve as a guide to getting maximum useful data out of limited observation networks and budgets. Exploring ways to augment SWE spatial coverage may additionally involve replacing point-based SWE data with alternative sources such as remote sensing techniques like Lidar (Painter et al., 2016) or leveraging gridded snow products like SnowCast (<http://www.snowcast.ca>; Vionnet et al., 2021a) (Mortimer et al., 2020).

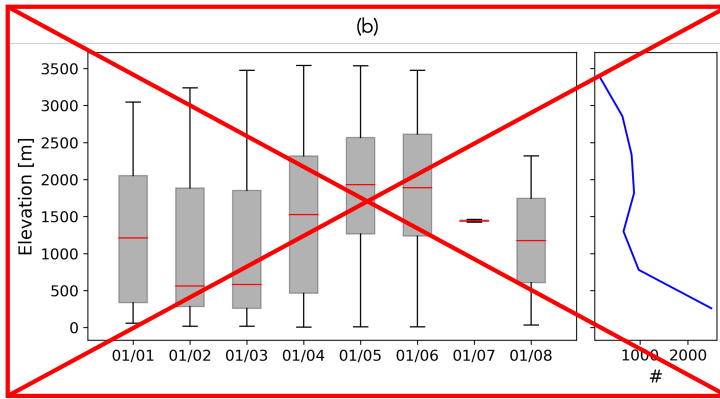
This discussion further leads to questions about how additional SWE measurements can improve the quality of the streamflow forecasts. There are instances where manual SWE measurements fail to accurately capture the peak snowpack (particularly

problematic in the absence of automatic snow measurements within the basin). On top of this, the forecasting strategy utilized here (i.e., initializing forecasts on the first of each month) may also miss the peak snowpack. To address this, exploring more frequent predictions, like initializing and updating forecasts in the middle of each month, could prove beneficial. Additional research aimed at enhancing snow surveying networks could concentrate on identifying station locations that are representative of the basin SWE at different dates. These specific sites could then be targeted for additional point measurements or continuous monitoring using snow pillows, snow scales, or snow depth sensors to ensure the comprehensive capture of mid-month peak SWE events.



**Figure 9.** (a) SWE content on the first day of each month between January 1<sup>st</sup> and September 1<sup>st</sup>. (b) SWE station elevations as a function of maximum SWE dates and line histogram of the elevation of SWE stations.





## 460 4.2 Forecasters

According to our second hypothesis, we expect higher hindcast quality for hindcasts with high antecedent SWE content and low precipitation during the hindcast target period in each basin (see Section 2.2.5). We quantify the impact of antecedent snowpack vs. future precipitation on the hindcast performance. Figure 10 shows the P/SWE ratio (see Section 2.2.5 for more information on its calculation) as a function of hindcast Fair CRPSS for each target period. As anticipated, for most target periods, the hindcast skill increases as the P/SWE ratio decreases. This suggests that the hindcasts are more skilful when the initialization date snowpack increases and/or when the target period precipitation proportion decreases. However, this relationship varies across different target periods. There is a stronger correlation (with statistical significance) for hindcasts generated for the target periods March 1<sup>st</sup> to September 30<sup>th</sup>, April 1<sup>st</sup> to September 30<sup>th</sup>, and May 1<sup>st</sup> to September 30<sup>th</sup>. Furthermore, this relationship does not hold for target periods August 1<sup>st</sup> to September 30<sup>th</sup> and September 1<sup>st</sup> to 30<sup>th</sup>.

465

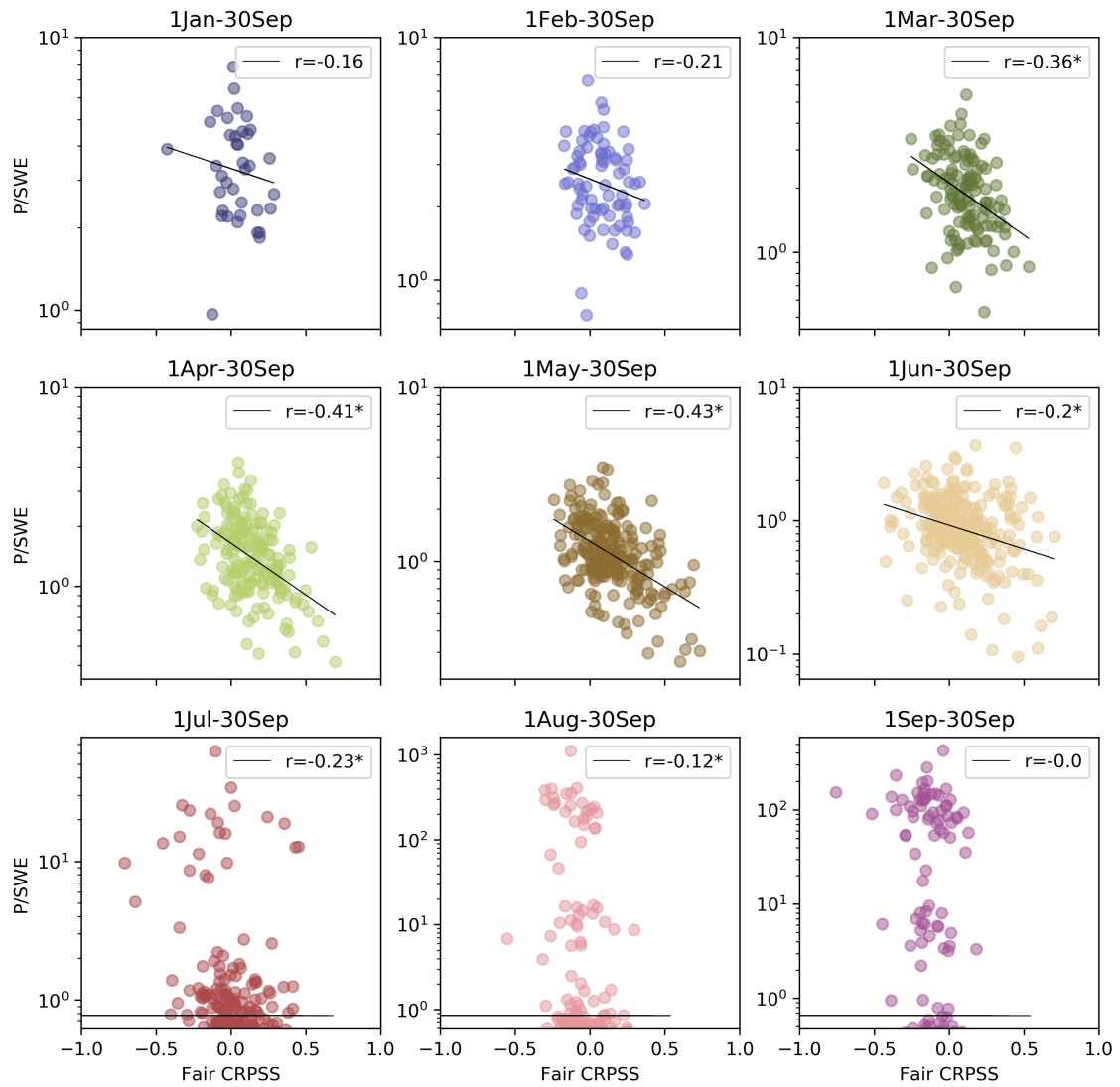
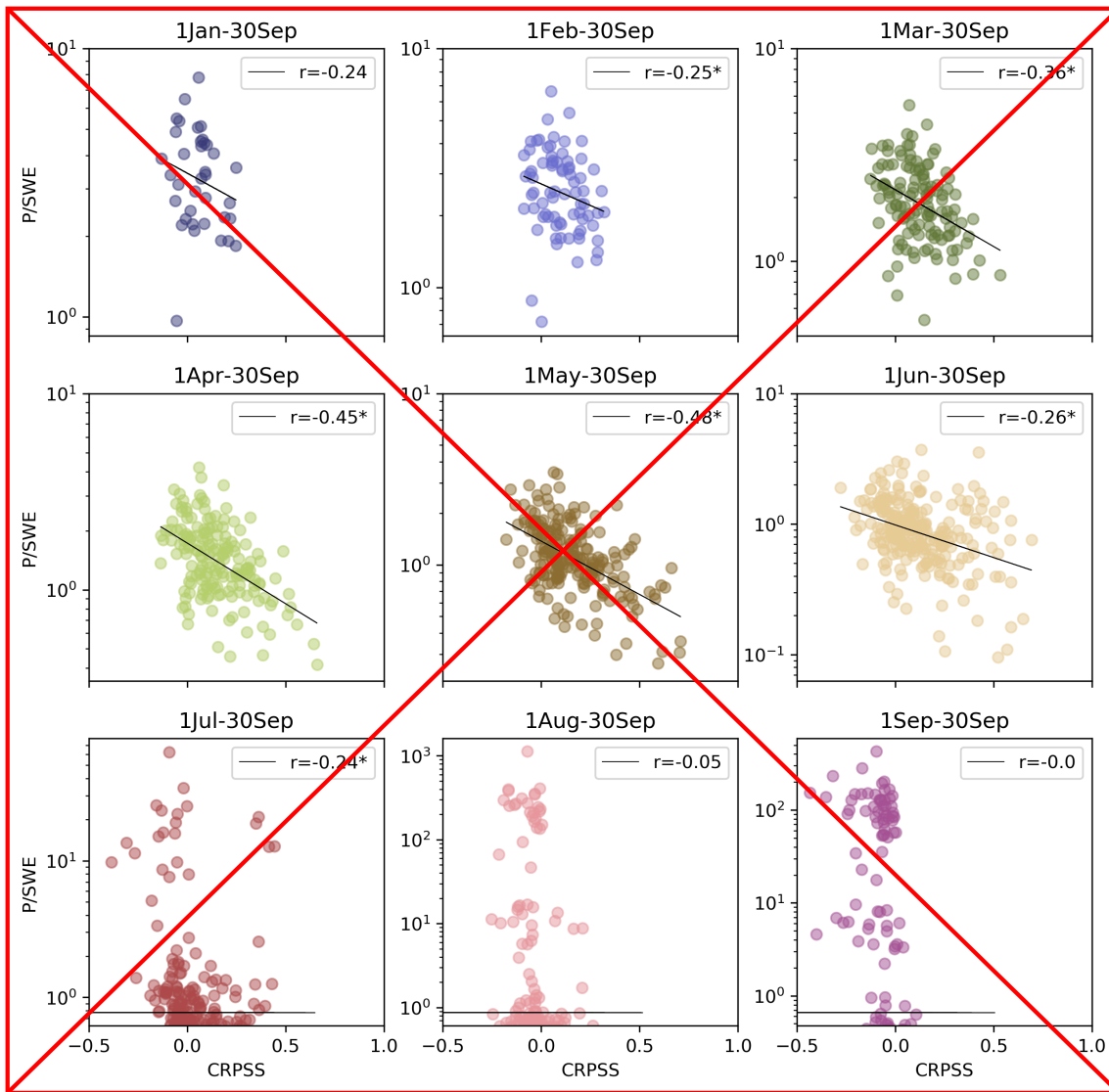


**Figure 10.** P/SWE as a function of hindcast Fair CRPSS for all hindcast initialization dates and all basins for each target period (subplots). Each point represents the result for a given basin and initialization date. The Pearson correlation coefficient ( $r$ ) is shown on the top right of each plot, where the asterisk denotes statistical significance at a 5% significance level.



470

This figure emphasizes the sensitivity of the results to the flow regime, raising concerns about potential loss of predictability with a changing (snow) climate. According to the Sixth Assessment Report of the Intergovernmental Panel on Climate Change (IPCC, 2021, 2022), snow extent, snow cover duration, and accumulated snowpack are virtually certain to decline in subarctic regions of North America. There is also a projected decrease in seasonal snow cover extent and mass in mid- to high-latitudes and at high elevations. Hale et al. (2023) report that the annual snow storage has decreased in over 25% of mountainous areas in western North America between 1950 and 2013, as a result of earlier snowmelt and rainfall in spring months, and declines in winter precipitation.

These changes are predicted to result in snow-related hydrological changes, including declines in snowmelt runoff (except in glacier-fed river basins where the opposite might be true on shorter timescales) (IPCC, 2021, 2022), more frequent rain-on-snow events at higher elevations (where seasonal snow cover persists) due to a shift from snowfall to rain (Musselman

480



et al., 2018), and consecutive snow drought years in western North America. Berghuijs et al. (2014) show that a change in the precipitation phase from snow to rain significantly decreases the mean streamflow within individual catchments of the contiguous USA. In snow-dominated regions globally, there is high confidence that peak flows associated with spring snowmelt will occur earlier in the year. This effect has already been documented by several studies that show that new record  
485 peak flows fall into time periods outside the nival window (Gillett et al., 2022). Burn and Whitfield (2023) additionally discuss an increasing frequency of rainfall-driven peaks and floods.

As a result of these changes, we expect that the relationships between SWE and streamflow will be affected, impacting the quality of snow-based streamflow forecasts in the future. Pagano et al. (2004) found that increasing hydrological variability in the western USA was partly responsible for the decline in water supply forecast skill.

490 The analysis presented here showcases a wide spectrum of predictability, where basins encompass diverse geographies and climates, ranging from purely nival regimes to mixed regimes. This spectrum of predictability can be appreciated in more depth in Fig. A7 in the Appendix. This offers a glimpse into the potential changes in predictability we may observe in the future. To tackle these questions more thoroughly, future research could look at the impact of snow climate on these results. Additionally, investigating different cross-validation approaches could be influential in maintaining forecast quality over time.

495 In the study by Zheng et al. (2018), inner mountain areas in the western USA, (dominated by snowmelt contribution,) showed longer streamflow predictability, while coastal areas, (dominated by rainfall contribution,) had shorter streamflow predictability. While we sub-selected river basins with a nival regime, we do also notice the influence of future unknown rainfall on these results (see Fig. 10). Figure 7 illustrates higher and longer predictability in interior and western North American river basins, contrasting with lower and shorter predictability in the north and in the east, which partly aligns with the findings of Zheng  
500 et al. (2018). However, further analysis is needed to identify spatial patterns in the hindcast skill and their relationships with the physical processes of runoff generation.

Climate predictors can add to the seasonal streamflow forecast skill available from SWE, especially for basins with strong teleconnections between large-scale climate and local meteorology on longer timescales (Wood et al., 2016; Mendoza et al., 2017). Furthermore, Slater and Villarini (2017) found precipitation variability to be crucial for modeling high flows, while  
505 antecedent wetness impacts low and median flows in the Midwestern USA. They also found that temperature enhances model fits during snowmelt or high evapotranspiration seasons. Lehner et al. (2017) found that the addition of temperature forecast information to operational seasonal streamflow predictions in snowmelt-driven basins within the southwest USA not only enhances the skill of streamflow forecasts but also contributes to mitigating errors in streamflow predictions caused by climate nonstationarity. Antecedent streamflow can also be a strong predictor of future streamflow, as shown by Veiga et al. (2014).

510 These variables might enhance predictability and warrant exploration. However, the predictability sources vary depending on the initialization date, predictand, basin location, and hydroclimatic features (Wood et al., 2016). Even within a small domain, the relative importance of predictors can differ (Mendoza et al., 2017), emphasizing the need for detailed analysis to put forward additional basin specific predictors. Tools like PyForecast (<https://github.com/usbr/PyForecast>) could aid in exploring additional predictors for accurate ensemble seasonal volume forecasts within specific river basins or regions using  
515 the workflow presented here.

Additionally, embracing more flexible yet physically accurate forecasting methods is a logical progression. Hybrid methods that combine the strengths of machine learning with process-based models grounded in our comprehension of physical processes emerge as a reasonable choice for enhancing predictability over longer timescales (Slater et al., 2023). In recent studies, Chang et al. (2023) demonstrated the extended predictability of subseasonal hydrological forecasts in Switzerland by incorporating large-scale atmospheric circulation information. Additionally, Hauswirth et al. (2023) introduced a flexible and efficient hybrid framework that utilized global seasonal forecasts as inputs to produce skilful location-specific seasonal forecast information.

### 4.3 Decision-makers

This study focused solely on forecasting streamflows in unregulated river basins, which may include river basins upstream of a regulation, such as a reservoir or an urbanized area. Regulation alters the relationship between the hydro-meteorological drivers of streamflow and streamflow. In those regulated river basins, it is however still valuable to predict streamflows upstream of the regulation (e.g., the inflows to a reservoir, streamflows upstream of a city, or of a regulated river segment), where predictability comes from upstream SWE stations, for water management decision-making downstream (e.g., for water supply management, hydropower generation, irrigation scheduling, early warnings of floods and droughts, riverine transportation). This methodology could additionally add value in regulated catchments where the naturalized flow is used for water management decision-making.

Forecast reliability plays a crucial role in facilitating risk-based decision-making (Zhao et al., 2016; Mendoza et al., 2017), for example for determining optimal water release volumes and schedules for hydropower generation and irrigation, or for issuing timely warnings of potential high or low flows. High forecast reliability in turn instills trust in the forecasts for informed decision-making (note that reliability is only one of many factors that contribute to users' trust). Insights from the analysis of a serious game conducted by Crochemore et al. (2021) underscore the importance of high reliability for decision-making. Notably, the study revealed that decision-makers considered high reliability crucial especially for risk-based decision-making in extreme years.

One of the distinguishing strengths of statistical forecasts, such as the ones generated here, over process-based forecasts lies in their ability to achieve high forecast reliability, stemming from the ensemble generation method employed. This aligns with the findings of Mendoza et al. (2017), who found that the regression-based forecasting methods they examined exhibited higher reliability than the process-based forecasting methods. For five case study sites across the USA Pacific Northwest, their regression-based methods achieved reliability index values ranging between 0.6 and nearly 1, while the reliability of the process-based ensemble streamflow prediction (ESP) hindcasts declined when approaching the April 1<sup>st</sup> initialization date, with an overall reliability index ranging between 0.4 and 0.9. Our approach yielded reliability index values comparable to those obtained from the statistical methods developed by Mendoza et al. (2017). Emerton et al. (2018) found that the process-based seasonal streamflow forecasts produced within the Global Flood Awareness System (GloFAS) had limited reliability globally, with some spatial variability.

A fundamental question that arises pertains to the temporal horizon within which decisions can be confidently made. To provide some initial insights for decision-making, we provide matrices showing the evolution of the forecasts' potential usefulness for predicting low and high flows within specific river basins with increasing lead time, considering the period of interest within each basin (Fig. A6 in the Appendix). However, the answer to this question is inherently user-specific, and depends on factors such as the choice of baseline, target periods, and specific events or thresholds of interest. To address these specific user requirements, further analysis is essential. This can be achieved by building on the provided codes, and tailoring the forecasting methodology to align with distinct user needs.

In the context of operational forecasting, forecast consistency is a critical aspect to ensure coherent decisions throughout the decision-making period. Considering the findings presented in this paper from an operational forecasting standpoint, a few methodological decisions may have affected the results. In this analysis, we conducted a PCA and established new models for each predictor-predictand combination and each year left out. We adopted a leave-one-out cross-validation approach due to limited data in certain basins, leveraging all available data to generate new hindcasts. It is important to acknowledge that this approach might introduce inconsistency from month to month and year to year (Garen, David C., 1992), as well as some artificial quality in the hindcast verification process (DelSole and Shukla, 2009). In operational scenarios, forecasters may opt to use pre-existing PC matrices and models to ensure forecast consistency and ensure smooth decision-making. However, this could be problematic in case of non-stationary input data (Shen et al., 2022). This topic warrants further attention.

#### 565 **4.4 Workflow developers**

Reproducibility of research in the water sciences is still very low (Stagge et al., 2019). This contributes to the typically slow transfer of research to operations. While journal policies are moving towards more open science (e.g., Blöschl et al., 2014; Clark et al., 2021a), such policies are not yet at the stage where full workflows must be published alongside a paper - though this seems a logical next step.

570 Building workflows that are both intuitive (i.e., that can represent our understanding of local hydro-meteorological processes; (Veiga et al., 2014)) and reproducible is essential to providing platforms for progressive and purposeful testing of new scientific advances, and to pave the way for applying research outcomes in practice. Furthermore, it fosters more equitable water research and education (Castronova et al., 2023).

575 However, it is important to acknowledge that the demands of scientific journals for open-source data and methods may sometimes conflict with the rapid and competitive nature of some environments, including academia. Striking a balance between open collaboration and maintaining a competitive edge poses challenges that the academic community must address. Explicitly acknowledging a researcher's commitment to transparency, reproducibility, and reusability of their work during merit reviews is one possible step forward.

580 The workflow developed as part of this study adheres to the principles of open and collaborative science, facilitated by its design (i.e., Jupyter Notebooks) and code-sharing (i.e., GitHub). In line with the recommendations by Knobon et al. (2022), our approach prioritizes clarity, modularity, and traceability in the workflow design. This enables users to easily adapt the workflow

for any river basin in the USGS or the WSC HYDAT datasets. Users have the flexibility to modify, enhance, or replace specific components of the workflow to suit their needs. Below is a non-exhaustive list of future research ideas.

- 585 – In Notebook 1, one could look into replacing the regime classification component of this workflow with an alternative method to identify basins with a nival regime (such as using the fraction of precipitation falling as snow).
- In Notebook 2, we set the end of the water year as the endpoint for all forecast target periods in all river basins. Yet, some of these river basins may experience late summer to early fall rainfall events. For example, river basins in the east which can be impacted by extratropical storms during that time of year and show a mixed hydrological regime (Burn et al., 2016). While we discarded most of these river basins through the strict regime classification/basin selection, it could be 590 that some of these river basins were retained, affecting the forecast quality.
- In Notebook 3,
  - future research could explore the impact of using different gap filling methods. An example is the various gap filling strategies explored by Tang et al. (2020a) for meteorological stations infilling to create the SCDNA dataset.
  - We used the SCDNA precipitation data for infilling, which does not distinguish between solid and liquid precipi- 595 tation. Additionally, the precipitation was accumulated during the entire water year and did not consider the onset of snowmelt. Both of these decisions could have led to lower correlations between the SWE and the cumulative precipitation to identify suitable donor stations.
  - The selection of SWE stations used as predictors could play a significant role in the forecast quality. To improve SWE sampling, future research may consider expanding the station selection to include those within a buffer of the 600 basin. Although this method was coded as part of the workflow, it was not implemented in this paper due to the need for a more comprehensive analysis of its impact on forecast quality.
  - Subsequent studies could investigate how various methodological choices influence the quality and the effectiveness of the gap filling, using the artificial gap filling function. This could involve examining the consequences of implementing a total maximum allowable gap length to sub-select stations, or adjusting the window used for the 605 gap filling through quantile mapping.
- In Notebook 4,
  - there was no established minimum threshold for the percentage of variance that PC1 should explain in order to be used as a predictor. In addition, although the ability to use additional PCs was also coded as part of the workflow, it was not further explored in this paper in order to avoid overfitting. There exist 610 various methodologies around stopping criteria for including predictors, such as the Bayesian information criterion (BIC), or regularization approaches that can lessen the risk of overfitting (Baker et al., 2020). Investigating the effects of using additional PCs could lead to valuable insights. For instance, it could provide a means to investigate whether this accounts for the consistently underestimated variability.

- 615 – Subsequent studies may explore a range of cross-validation strategies (e.g., sample-splitting, increasing the number of omitted years, or excluding extreme years from the training dataset), to assess how they affect the quality of the generated hindcasts.

## 5 Conclusions

We have developed a systematic and reproducible data-driven workflow for probabilistic seasonal streamflow forecasting in snow-fed river basins across North America, including Canada and the USA. This structured workflow consists of five essential steps: 1) Regime classification and basins selection, 2) Streamflow pre-processing, 3) SWE pre-processing, 4) Forecasting, and 5) Hindcast verification. This methodology was applied to 75 basins characterized by a nival (snowmelt-driven) regime and limited regulation across diverse North American geographies and climates. The input data, spanning from 1979 to 2021, includes SWE (predictor), precipitation (for gap filling), and streamflow (predictand) station data. The ensemble hindcasts were generated monthly, with initialization dates ranging from January 1<sup>st</sup> to September 1<sup>st</sup>, and target periods January 1<sup>st</sup> - September 30<sup>th</sup>, February 1<sup>st</sup> - September 30<sup>th</sup>, and so on. We analyze the hindcasts using deterministic metrics (i.e., the KGE" and its decomposition to measure correlation, bias and variability) and probabilistic metrics (i.e., the reliability index, Fair CRPSS, and ROC AUC, to measure reliability, skill and potential usefulness, respectively). The insights derived from this comprehensive analysis are invaluable for snow monitoring experts, forecasters, decision-makers, and workflow developers.

Key findings include:

- 630 – **For snow monitoring experts:** Late-season snowpack (i.e., after April 1<sup>st</sup>) holds significant predictability for spring/summer volumes. Thus, capturing snowpack beyond the peak period is crucial for skilful predictions.
- **For forecasters:** Higher hindcast skill is achievable using this forecasting approach for target periods when basins exhibit high antecedent SWE content and low precipitation during the forecast period. In many river basins and times of year, SWE is not a key predictor. Therefore, an optimal approach should leverage climate predictors to achieve a more comprehensive balance between the initial conditions and meteorological forcings that contribute to the predictability of runoff.
- 635 – **For decision-makers:** This statistical forecasting approach, not unlike other statistical forecasting approaches, can generate ensemble hindcasts with that are statistically reliability reliable. Moreover, for all periods of interest up to and including June 1<sup>st</sup> to September 30<sup>th</sup>, we can predict lower than normal and higher than normal streamflows with up to five months lead time.
- 640 – **For workflow developers:** The developed workflow, shared as Jupyter Notebooks on GitHub, follows the principles of open and collaborative science. Its design is clear, modular, traceable, intuitive, and reproducible. This in turn facilitates applications in other cold regions, and the advancement of methods based on the benchmark provided. We invite others to build upon this workflow and have outlined potential improvements in Section 4.4.

645 This study contributes to the existing research by: 1) expanding the spatial scope to encompass both Canada and the USA,  
2) creating a completely open and reproducible workflow, and 3) offering practical guidance for diverse users.

*Code and data availability.* The Python codes used to generate all hindcasts analyzed in this paper are available on Zenodo (Arnal et al., 2023b, v0.9.0). The release additionally contains compiled datasets of the basin shapefiles and the daily streamflow observations used, described in more detail in the associated readme. A user-friendly version of the FROSTBYTE workflow is available on GitHub (Arnal et al.,  
650 2023a, v0.9.0), with sample data for two river basins to support reproducibility.

*Author contributions.* LA designed the workflow with the guidance of MC, AP, VV, VF, PW, DC, and AW. DC contributed to the development of the workflow GitHub repository. MC, VV and WK downloaded parts of the input data to the workflow. LA generated all hindcasts evaluated in this paper. LA prepared the manuscript with contributions from all co-authors.

*Competing interests.* The authors declare that they have no conflict of interest.

655 *Acknowledgements.* The authors acknowledge funding support from Environment and Climate Change Canada (ECCC), from the Canada First Research Excellence Fund's Global Water Futures program, and from NOAA CIROH as well as funding provided by the National Oceanic and Atmospheric Administration (NOAA), awarded to the Cooperative Institute for Research on Hydrology (CIROH) through the NOAA Cooperative Agreement with The University of Alabama, NA22NWS4320003. David Casson was partly funded by Deltares Strategic Research under the Dutch Subsidy for Institutes for Applied Research. Andrew Wood is supported by Reclamation under Interagency  
660 Agreements R21PG00095 and R22PG00035, by the U.S. Army Corps of Engineers Climate Preparedness and Resilience Program, and by NOAA CIROH under subaward A22-0310-S001-A02.

We would like to specifically thank the following people for their guidance throughout the workflow and manuscript preparation, in no specific order:

- 665 – Khaled Akhtar, Evan Friesenhan, Jennifer Nafziger, and other forecasters from the Government of Alberta in Edmonton, for discussions on streamflow forecasting and local challenges.
- Alex Cebulski, Dennis Rollag, and Marina Tait for a discussion on snow surveying.
- Pablo Mendoza for discussions around the hindcast evaluation.
- Guoqiang Tang, Kasra Keshavarz, and Shervan Gharari for data and example codes.
- Colleen Mortimer for compiling SWE data for New England (USA) used in this study.
- 670 – Alida Thiombiano for a revision of the SWE gap filling script.
- The handling editor, Wouter Buytaert, and two anonymous referees for their helpful comments during the review process of our manuscript.

We additionally acknowledge the contribution of SWE data by the Ministère de l'Environnement, de la Lutte contre les changements climatiques, de la Faune et des Parcs (MELCC, 2019).

675 The authors acknowledge that collectively they reside on traditional territories of the peoples of Treaties 6 and 7, which  
include the Cree, the Haudenosaunee, the Ktunaxa, the Mohawk, the Niitsitapi (Blackfoot Confederacy, comprised of the  
Siksika, the Piikani, and the Kainai First Nations), the Stoney Nakoda (including Chiniki, Bearspaw, and Goodstoney First  
Nations), and the Tsut'ina First Nation, on the homelands of the Métis, on the ancestral homelands of the Cheyenne, Arapaho,  
Ute and many other Native American nations, as well as on unceded Indigenous lands of which the Kanien'kehá:ka Nation are  
680 the custodians. The authors thank these nations for their care and stewardship over this land and water and pay their respect  
to the ancestors of these places. It is hoped that this article helps to improve river flow forecasting worldwide to protect all its  
communities and people.

## Appendix A: Additional figures

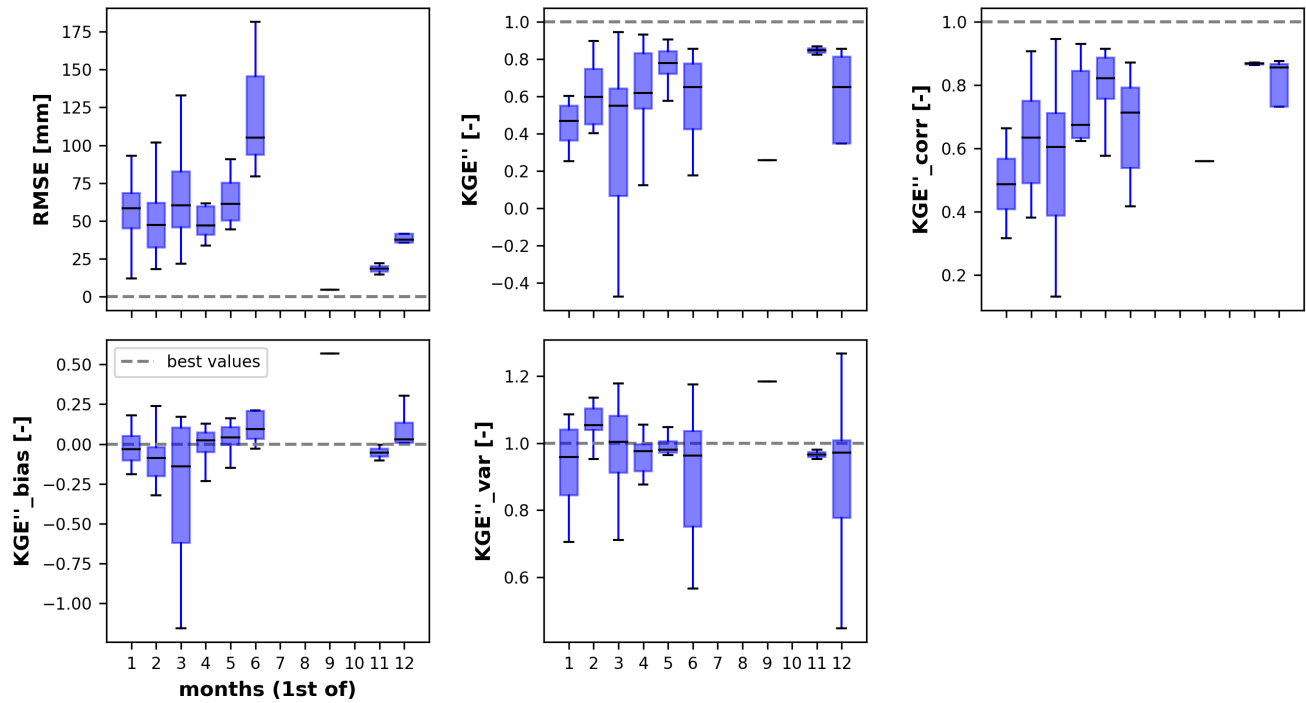


**Figure A1.** Performance metrics obtained from the artificial gap filling step for the Bow River at Banff (Alberta, Canada). The boxplots contain results for all SWE stations within the river basin.



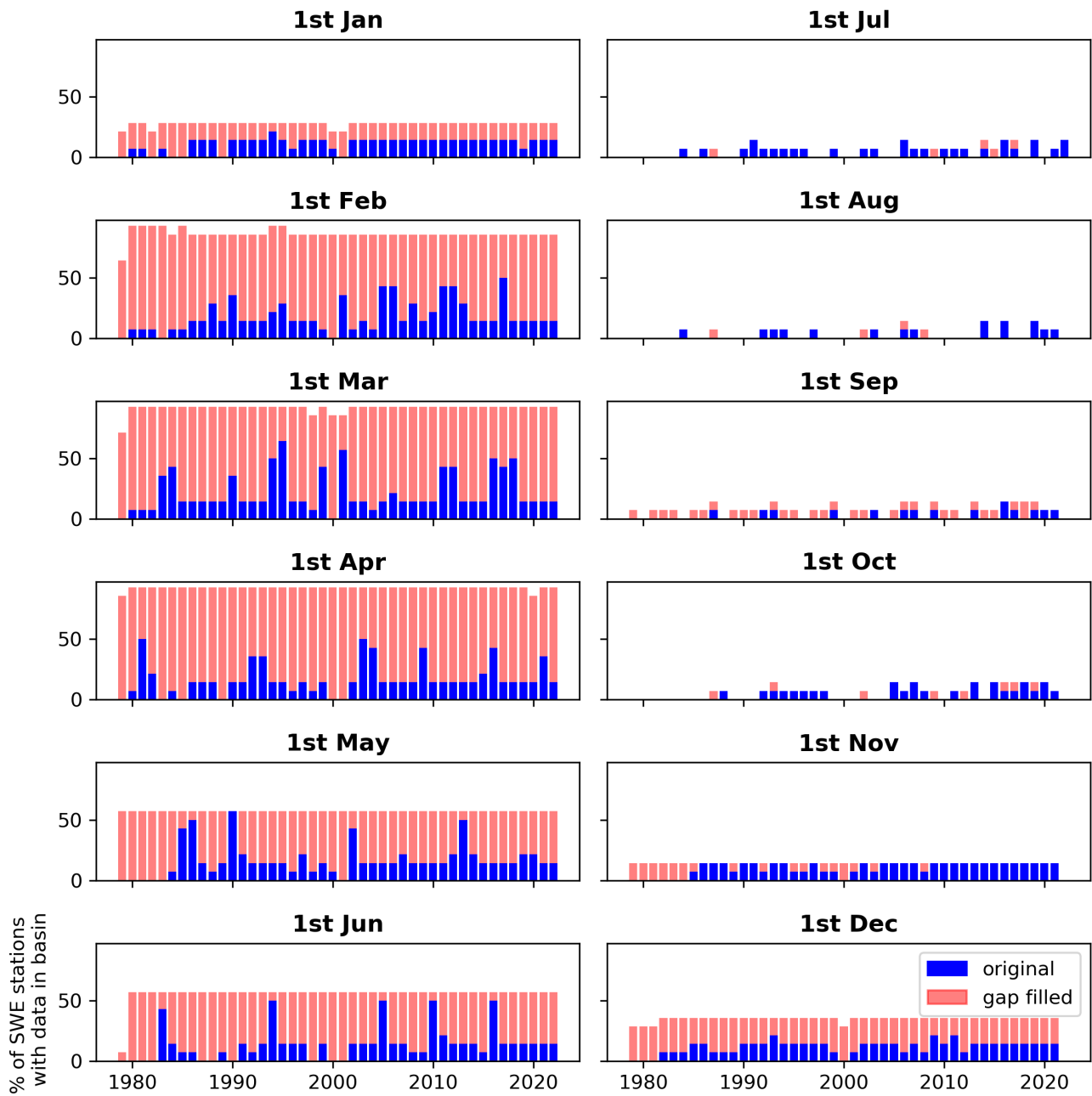


**Figure A2.** Time series of the availability of SWE station data on the first day of each month (subplots) before and after gap filling for the Bow River at Banff (Alberta, Canada).

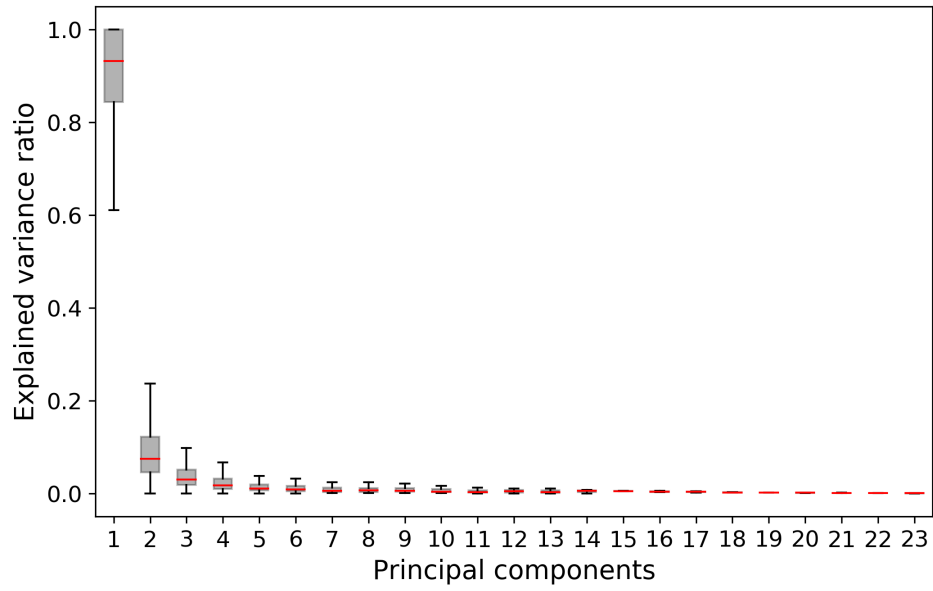


**Figure A3.** Explained variance for all SWE principal components. The boxplots display values for all hindcast initialization dates and basins.

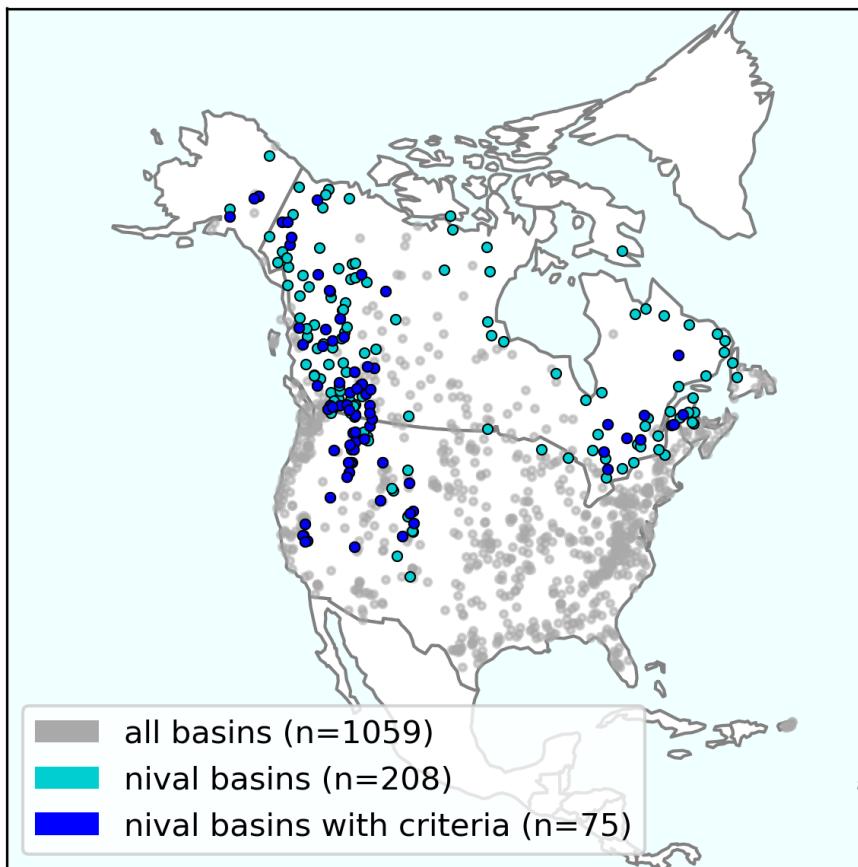


**Figure A4.** Map of all North American basins with data for the period 1979–2021 and with limited regulation (grey), identified nival basins (turquoise), and the subset of nival basins meeting the data requirements for the forecasting analysis presented in this paper (dark blue).

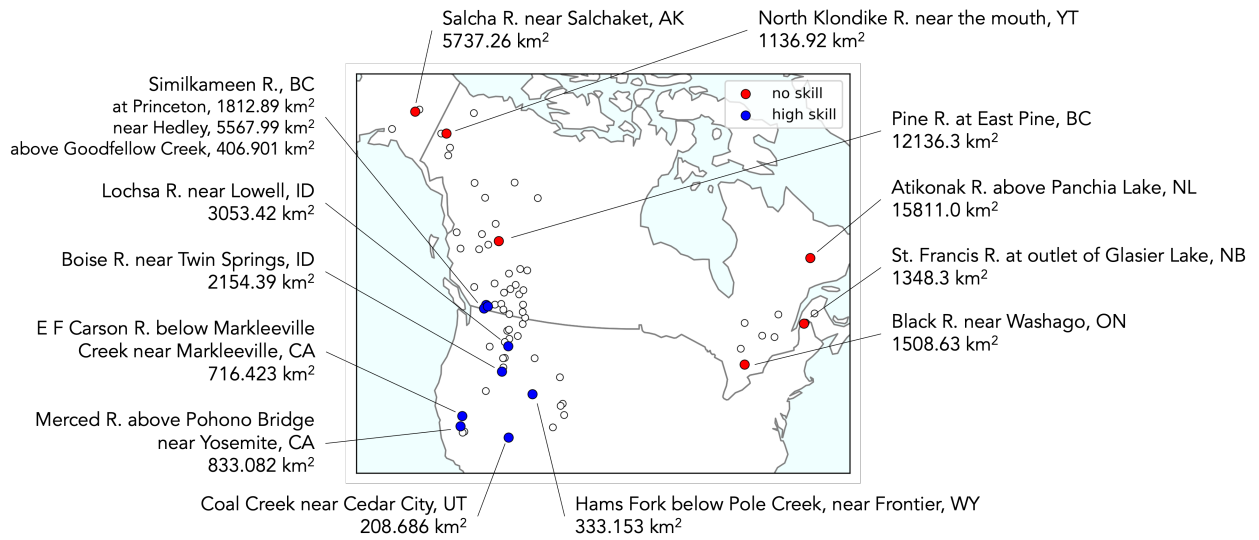


**Figure A5.** Map highlighting river basins in which skill consistently falls below zero (Fair CRPSS < 0 across all lead months for the basin's target period of interest; red) and those exhibiting consistently high skill (Fair CRPSS ≥ 0.5 across all lead months for the basin's target period of interest; blue).

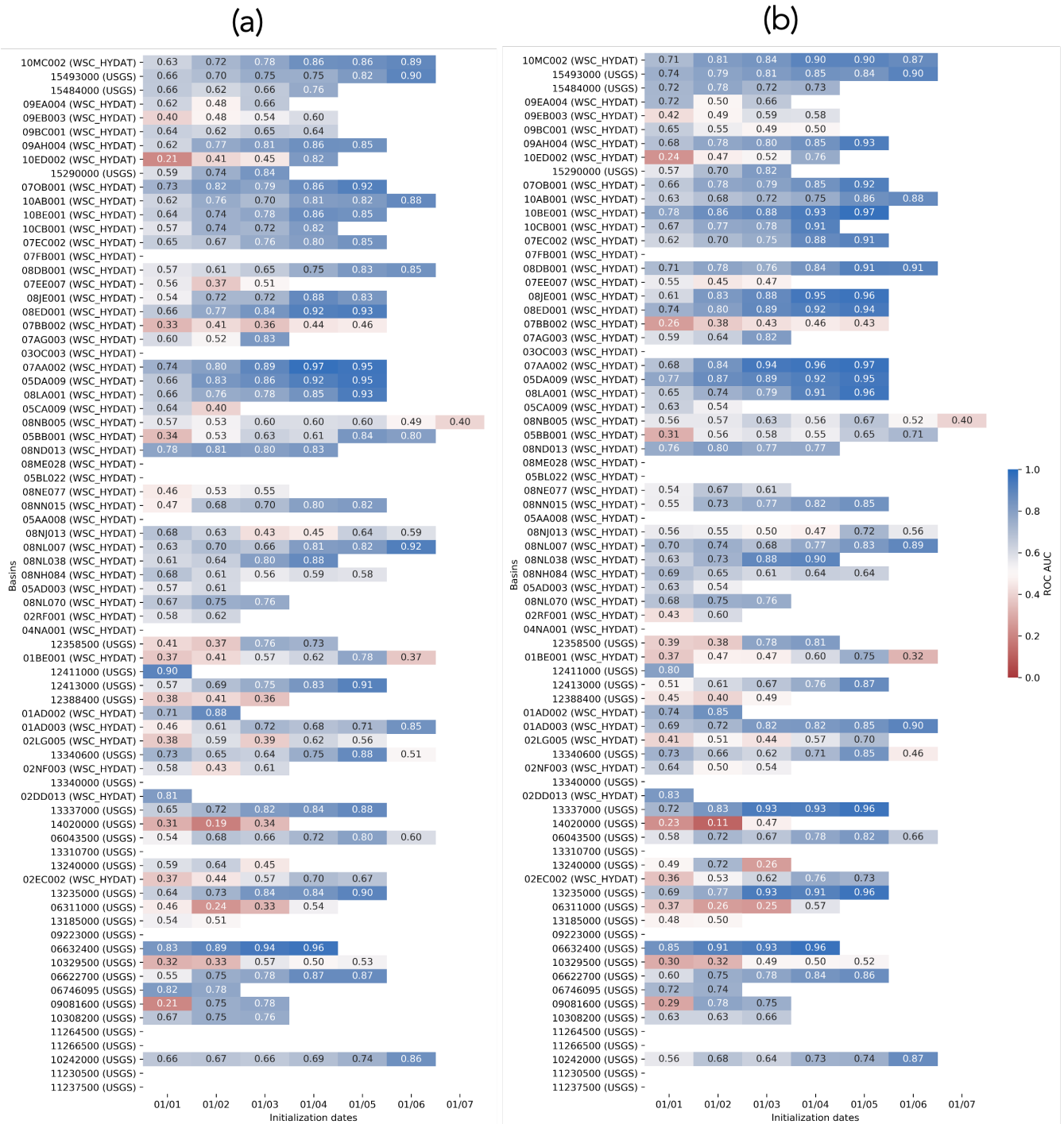


**Figure A6.** Hindcast ROC AUC for each basin as a function of initialization dates (a) for flows below the climatology lower tercile and (b) for flows above the climatology upper tercile (right). Results are shown only for each basin’s period of interest. Basins are ordered from North to South, based on their latitudes. Blue colours show potential useful hindcasts and red colours show hindcasts with no skill.

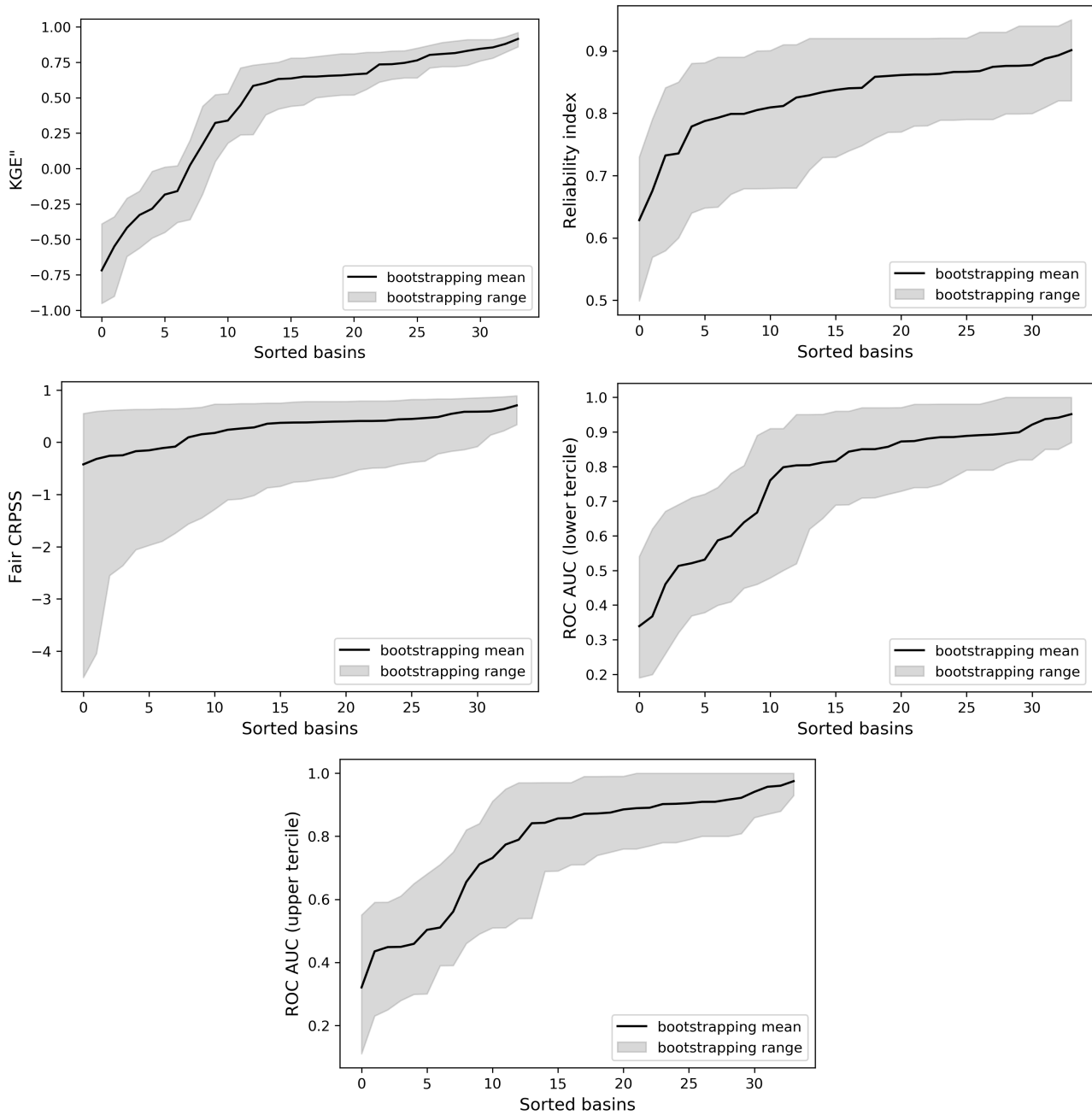
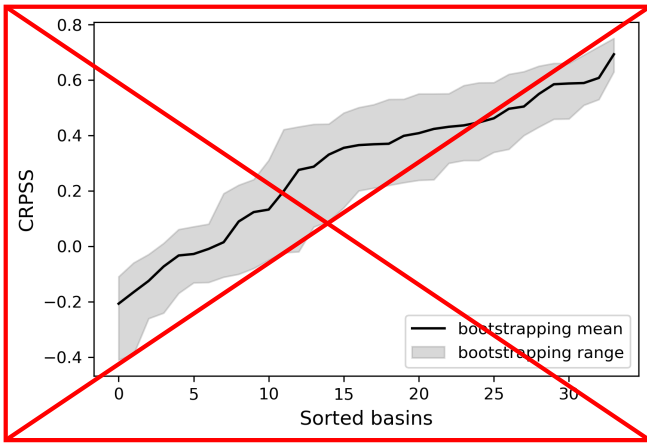


**Figure A7.** Bootstrapping mean and range ( $5^{th}$  to  $95^{th}$  percentiles) for various metrics across the selected nival river basins (sorted from lowest to highest mean metric value). Results are shown for June 1<sup>st</sup> to September 30<sup>th</sup> hindcasts generated on June 1<sup>st</sup> for illustrative purposes.



## 685 Appendix B: Circular statistics

The equations used for the regime classification were taken from Burn et al. (2010). The date of occurrence of an event ( $i$ ) is defined by converting the Julian date to an angular value ( $\theta_i$ ; in radians), using the formula:

$$\theta_i = (JulianDate_i) \left( \frac{2\pi}{lenyr} \right) \quad (B1)$$

where  $lenyr$  is the number of days in a year.

690 From a sample of  $n$  events, we can find the x- and y-coordinates of the mean date with the following formulas:

$$\bar{x} = \frac{1}{n} \sum_{i=1}^n \cos\theta_i \quad (B2)$$

$$\bar{y} = \frac{1}{n} \sum_{i=1}^n \sin\theta_i \quad (B3)$$

The mean date ( $MD$ ), or average date of occurrence of all events  $i$ , can then be obtained with:

$$MD = \tan^{-1} \left( \frac{\bar{y}}{\bar{x}} \right) \left( \frac{lenyr}{2\pi} \right) \quad (B4)$$

695 Finally, the regularity ( $\bar{r}$ ) of the  $n$  event occurrences can be determined with the formula:

$$\bar{r} = \sqrt{\bar{x}^2 + \bar{y}^2} \quad (B5)$$

where  $\bar{r}$  is a dimensionless measure of the spread in the dates of occurrences of the  $n$  events, which varies from zero to one. Larger values indicate a higher level of regularity.

## Appendix C: KGE" decomposition

700 The equations for the components of the KGE" were taken from Clark et al. (2021b). The bias ratio ( $\beta$ ) is:

$$\beta = \frac{(\mu_s - \mu_o)^2}{\sigma_o^2} \quad (C1)$$

where  $\mu_s$  is the mean of the simulations,  $\mu_o$  is the mean of the observations, and  $\sigma_o^2$  is the variance of the observations.  $\beta$  has a perfect score of zero.

The variability ratio ( $\alpha$ ) is:

$$705 \quad \alpha = \frac{\sigma_s}{\sigma_o} \quad (C2)$$

$\alpha$  has a perfect score of one.

The correlation ( $\rho$ ) is the Pearson correlation between the simulations and the observations, and has a perfect score of one.



## Appendix D: SWE and precipitation statistics

We computed the Snow Water Equivalent (SWE) content historical median for each initialization date  $i$  and each SWE station  $s$  using the formula:

$$SWEcontent_{i,s} = med\left(\frac{SWE_{i,wy,s}}{max(SWE)_{wy,s}} \times 100\right) \quad (D1)$$

where  $SWE_{i,wy,s}$  is the SWE on initialization date  $i$  within water year  $wy$  and for SWE station  $s$ , and  $max(SWE)_{wy,s}$  is the maximum SWE for water year  $wy$  for SWE station  $s$ .

To determine the precipitation to SWE ratio, we first calculated the basin mean cumulative precipitation historical median for each target period  $t$  and each nival basin  $b$  with:

$$Pstats_{t,b} = \frac{1}{n} \sum_{s=1}^n med(Pcumul_{t,s}) \quad (D2)$$

where  $n$  is the total number of precipitation stations  $s$  in basin  $b$ .

Next, we calculated the basin mean SWE historical median for each initialization date  $i$  and each nival basin  $b$  with:

$$SWEstats_{i,b} = \frac{1}{n} \sum_{s=1}^n med(SWE_{i,s}) \quad (D3)$$

where  $n$  is the total number of SWE stations  $s$  in basin  $b$ .

Finally, the precipitation to SWE ratio was determined for each combination of initialization date  $i$ , target period  $t$ , and nival basin  $b$  with:

$$P/SWE_{t,i,b} = \frac{Pstats_{t,b}}{SWEstats_{i,b}} \quad (D4)$$

The precipitation to SWE ratio ranges between  $-\infty$  and  $+\infty$ .

## 725 **References**

- Arnal, L., Cloke, H. L., Stephens, E., Wetterhall, F., Prudhomme, C., Neumann, J., Krzeminski, B., and Pappenberger, F.: Skilful seasonal forecasts of streamflow over Europe?, *Hydrology and Earth System Sciences*, 22, 2057–2072, <https://doi.org/https://doi.org/10.5194/hess-22-2057-2018>, 2018.
- 730 Arnal, L., Casson, D. R., Clark, M. P., and Thiombiano, A. N.: FROSTBYTE: Forecasting River Outlooks from Snow Timeseries: Building Yearly Targeted Ensembles, <https://github.com/CH-Earth/FROSTBYTE>, 2023a.
- Arnal, L., Vionnet, V., and Clark, M.: FROSTBYTE: Forecasting River Outlooks from Snow Timeseries: Building Yearly Targeted Ensembles, <https://doi.org/10.5281/zenodo.10310683>, 2023b.
- Baker, S. A., Wood, A. W., and Rajagopalan, B.: Application of Postprocessing to Watershed-Scale Subseasonal Climate Forecasts over the Contiguous United States, *Journal of Hydrometeorology*, 21, 971–987, <https://doi.org/10.1175/JHM-D-19-0155.1>, 2020.
- 735 Berghuijs, W. R., Woods, R. A., and Hrachowitz, M.: A precipitation shift from snow towards rain leads to a decrease in streamflow, *Nature Climate Change*, 4, 583–586, <https://doi.org/10.1038/nclimate2246>, 2014.
- Blöschl, G., Bárdossy, A., Koutsoyiannis, D., Kundzewicz, Z. W., Littlewood, I., Montanari, A., and Savenije, H.: On the future of journal publications in hydrology, *Water Resources Research*, 50, 2795–2797, <https://doi.org/10.1002/2014WR015613>, 2014.
- Burn, D. H. and Whitfield, P. H.: Changes in cold region flood regimes inferred from long-record reference gauging stations, *Water Resources Research*, 53, 2643–2658, <https://doi.org/10.1002/2016WR020108>, 2017.
- 740 Burn, D. H. and Whitfield, P. H.: Climate related changes to flood regimes show an increasing rainfall influence, *Journal of Hydrology*, 617, 129 075, <https://doi.org/10.1016/j.jhydrol.2023.129075>, 2023.
- Burn, D. H., Sharif, M., and Zhang, K.: Detection of trends in hydrological extremes for Canadian watersheds, *Hydrological Processes*, 24, 1781–1790, <https://doi.org/10.1002/hyp.7625>, 2010.
- 745 Burn, D. H., Whitfield, P. H., and Sharif, M.: Identification of changes in floods and flood regimes in Canada using a peaks over threshold approach: Changes in Floods and Flood Regimes in Canada Based on a POT Approach, *Hydrological Processes*, 30, 3303–3314, <https://doi.org/10.1002/hyp.10861>, 2016.
- Cartwright, K., Hopkinson, C., Kienzle, S., and Rood, S. B.: Evaluation of temporal consistency of snow depth drivers of a Rocky Mountain watershed in southern Alberta, *Hydrological Processes*, 34, 4996–5012, <https://doi.org/10.1002/hyp.13920>, 2020.
- 750 Castronova, A. M., Nassar, A., Knoben, W., Fienen, M. N., Arnal, L., and Clark, M.: Community Cloud Computing Infrastructure to Support Equitable Water Research and Education, *Groundwater*, 61, 612–616, <https://doi.org/10.1111/gwat.13337>, 2023.
- Chang, A. Y.-Y., Bogner, K., Grams, C. M., Monhart, S., Domeisen, D. I. V., and Zappa, M.: Exploring the Use of European Weather Regimes for Improving User-Relevant Hydrological Forecasts at the Subseasonal Scale in Switzerland, *Journal of Hydrometeorology*, 24, 1597–1617, <https://doi.org/10.1175/JHM-D-21-0245.1>, 2023.
- 755 Cho, E., Jacobs, J. M., and Vuyovich, C. M.: The Value of Long-Term (40 years) Airborne Gamma Radiation SWE Record for Evaluating Three Observation-Based Gridded SWE Data Sets by Seasonal Snow and Land Cover Classifications, *Water Resources Research*, 56, e2019WR025 813, <https://doi.org/10.1029/2019WR025813>, 2020.
- Clark, M. P., Luce, C. H., AghaKouchak, A., Berghuijs, W., David, C. H., Duan, Q., Ge, S., Van Meerveld, I., Zheng, C., Parlange, M. B., and Tyler, S. W.: Open Science: Open Data, Open Models, . . . and Open Publications?, *Water Resources Research*, 57, e2020WR029 480, <https://doi.org/10.1029/2020WR029480>, 2021a.
- 760

- Clark, M. P., Vogel, R. M., Lamontagne, J. R., Mizukami, N., Knoben, W. J. M., Tang, G., Gharari, S., Freer, J. E., Whitfield, P. H., Shook, K. R., and Papalexiou, S. M.: The Abuse of Popular Performance Metrics in Hydrologic Modeling, *Water Resources Research*, 57, <https://doi.org/10.1029/2020WR029001>, 2021b.
- Court, A.: Measures of streamflow timing, *Journal of Geophysical Research*, 67, 4335–4339, <https://doi.org/10.1029/JZ067i011p04335>, 1962.
- Crochemore, L., Cantone, C., Pechlivanidis, I. G., and Photiadou, C. S.: How Does Seasonal Forecast Performance Influence Decision-Making? Insights from a Serious Game, *Bulletin of the American Meteorological Society*, 102, E1682–E1699, <https://doi.org/10.1175/BAMS-D-20-0169.1>, 2021.
- Delgado-Ramos, F. and Hervás-Gamez, C.: Simple and Low-Cost Procedure for Monthly and Yearly Streamflow Forecasts during the Current Hydrological Year, *Water*, 10, <https://doi.org/https://doi.org/10.3390/w10081038>, 2018.
- DelSole, T. and Shukla, J.: Artificial Skill due to Predictor Screening, *Journal of Climate*, 22, 331–345, <https://doi.org/10.1175/2008JCLI2414.1>, 2009.
- Dyer, J.: Snow depth and streamflow relationships in large North American watersheds, *Journal of Geophysical Research: Atmospheres*, 113, <https://doi.org/https://doi.org/10.1029/2008JD010031>, 2008.
- ECCC: National Water Data Archive: HYDAT, <https://www.canada.ca/en/environment-climate-change/services/water-overview/quantity/monitoring/survey/data-products-services/national-archive-hydat.html>, last accessed: 2023-12-05, 2018.
- ECCC: Reference Hydrometric Basin Network, <https://www.canada.ca/en/environment-climate-change/services/water-overview/quantity/monitoring/survey/data-products-services/reference-hydrometric-basin-network.html>, last accessed: 2023-12-05, 2021.
- Emerton, R., Zsoter, E., Arnal, L., Cloke, H. L., Muraro, D., Prudhomme, C., Stephens, E. M., Salamon, P., and Pappenberger, F.: Developing a global operational seasonal hydro-meteorological forecasting system: GloFAS-Seasonal v1.0, *Geoscientific Model Development*, 11, 3327–3346, <https://doi.org/https://doi.org/10.5194/gmd-11-3327-2018>, 2018.
- Falcone, J.: GAGES-II: Geospatial Attributes of Gages for Evaluating Streamflow: U.S. Geological Survey data release, <https://doi.org/10.5066/P96CPHOT>, 2011.
- Ferro, C. A. T.: Fair scores for ensemble forecasts: Fair Scores for Ensemble Forecasts, *Quarterly Journal of the Royal Meteorological Society*, 140, 1917–1923, <https://doi.org/10.1002/qj.2270>, 2014.
- Ferro, C. A. T., Richardson, D. S., and Weigel, A. P.: On the effect of ensemble size on the discrete and continuous ranked probability scores, *Meteorological Applications*, 15, 19–24, <https://doi.org/10.1002/met.45>, 2008.
- Fleming, S. W. and Garen, D. C.: Simplified Cross-Validation in Principal Component Regression (PCR) and PCR-Like Machine Learning for Water Supply Forecasting, *JAWRA Journal of the American Water Resources Association*, 58, 517–524, <https://doi.org/10.1111/1752-1688.13007>, 2022.
- Fleming, S. W., Garen, D. C., Goodbody, A. G., McCarthy, C. S., and Landers, L. C.: Assessing the new Natural Resources Conservation Service water supply forecast model for the American West: A challenging test of explainable, automated, ensemble artificial intelligence, *Journal of Hydrology*, 602, 126 782, <https://doi.org/10.1016/j.jhydrol.2021.126782>, 2021.
- Garen, David C.: Improved Techniques in Regression-Based Streamflow Volume Forecasting, *Journal of Water Resources Planning and Management*, 118, 654–670, [https://doi.org/10.1061/\(ASCE\)0733-9496\(1992\)118:6\(654\)](https://doi.org/10.1061/(ASCE)0733-9496(1992)118:6(654)), 1992.
- Gharari, S., Keshavarz, K., Knoben, W. J. M., Tang, G., and Clark, M. P.: EASYMORE: A Python package to streamline the remapping of variables for Earth System models, *SoftwareX*, 24, 101 547, <https://doi.org/10.1016/j.softx.2023.101547>, 2023.

- 800 Gillett, N. P., Cannon, A. J., Malinina, E., Schnorbus, M., Anslow, F., Sun, Q., Kirchmeier-Young, M., Zwiers, F., Seiler, C., Zhang, X., Flato, G., Wan, H., Li, G., and Castellan, A.: Human influence on the 2021 British Columbia floods, *Weather and Climate Extremes*, 36, 100441, <https://doi.org/10.1016/j.wace.2022.100441>, 2022.
- Gobena, A. K. and Gan, T. Y.: Statistical Ensemble Seasonal Streamflow Forecasting in the South Saskatchewan River Basin by a Modified Nearest Neighbors Resampling, *Journal of Hydrologic Engineering*, 14, 628–639, [https://doi.org/10.1061/\(ASCE\)HE.1943-5584.0000021](https://doi.org/10.1061/(ASCE)HE.1943-5584.0000021), 2009.
- 805 Grünewald, T., Bühler, Y., and Lehning, M.: Elevation dependency of mountain snow depth, *The Cryosphere*, 8, 2381–2394, <https://doi.org/10.5194/tc-8-2381-2014>, 2014.
- Gupta, H. V., Kling, H., Yilmaz, K. K., and Martinez, G. F.: Decomposition of the mean squared error and NSE performance criteria: Implications for improving hydrological modelling, *Journal of Hydrology*, 377, 80–91, <https://doi.org/10.1016/j.jhydrol.2009.08.003>, 2009.
- Hale, K. E., Jennings, K. S., Musselman, K. N., Livneh, B., and Molotch, N. P.: Recent decreases in snow water storage in western North America, *Communications Earth & Environment*, 4, 170, <https://doi.org/10.1038/s43247-023-00751-3>, 2023.
- 810 Hauswirth, S. M., Bierkens, M. F. P., Beijk, V., and Wanders, N.: The suitability of a seasonal ensemble hybrid framework including data-driven approaches for hydrological forecasting, *Hydrology and Earth System Sciences*, 27, 501–517, <https://doi.org/10.5194/hess-27-501-2023>, 2023.
- Hersbach, H.: Decomposition of the Continuous Ranked Probability Score for Ensemble Prediction Systems, *Weather and Forecasting*, 15, 559–570, [https://doi.org/10.1175/1520-0434\(2000\)015<0559:DOTCRP>2.0.CO;2](https://doi.org/10.1175/1520-0434(2000)015<0559:DOTCRP>2.0.CO;2), 2000.
- 815 Hodson, T. O. and Hariharan, J. A.: dataretrieval (python): a Python package for discovering and retrieving water data available from Federal hydrologic web services, <https://doi.org/10.5066/P94I5TX3>, 2023.
- Immerzeel, W. W., Lutz, A. F., Andrade, M., Bahl, A., Biemans, H., Bolch, T., Hyde, S., Brumby, S., Davies, B. J., Elmore, A. C., Emmer, A., Feng, M., Fernández, A., Haritashya, U., Kargel, J. S., Koppes, M., Kraaijenbrink, P. D. A., Kulkarni, A. V., Mayewski, P. A., Nepal, S., Pacheco, P., Painter, T. H., Pellicciotti, F., Rajaram, H., Rupper, S., Sinisalo, A., Shrestha, A. B., Viviroli, D., Wada, Y., Xiao, C., Yao, 820 T., and Baillie, J. E. M.: Importance and vulnerability of the world’s water towers, *Nature*, 577, 364–369, <https://doi.org/10.1038/s41586-019-1822-y>, 2020.
- IPCC: *Climate Change 2021 – The Physical Science Basis: Working Group I Contribution to the Sixth Assessment Report of the Intergovernmental Panel on Climate Change*, Cambridge University Press, 1 edn., ISBN 978-1-00-915789-6, <https://doi.org/10.1017/9781009157896>, 2021.
- 825 IPCC: *Climate Change 2022 – Impacts, Adaptation and Vulnerability: Working Group II Contribution to the Sixth Assessment Report of the Intergovernmental Panel on Climate Change*, Cambridge University Press, 1 edn., ISBN 978-1-00-932584-4, <https://doi.org/10.1017/9781009325844>, 2022.
- Knoben, W. J. M., Clark, M. P., Bales, J., Bennett, A., Gharari, S., Marsh, C. B., Nijssen, B., Pietroniro, A., Spiteri, R. J., Tang, G., Tarboton, D. G., and Wood, A. W.: Community Workflows to Advance Reproducibility in Hydrologic Modeling: Separating Model- 830 Agnostic and Model-Specific Configuration Steps in Applications of Large-Domain Hydrologic Models, *Water Resources Research*, 58, <https://doi.org/10.1029/2021WR031753>, 2022.
- Lehner, F., Wood, A. W., Llewellyn, D., Blatchford, D. B., Goodbody, A. G., and Pappenberger, F.: Mitigating the Impacts of Climate Nonstationarity on Seasonal Streamflow Predictability in the U.S. Southwest, *Geophysical Research Letters*, 44, <https://doi.org/10.1002/2017GL076043>, 2017.

- 835 Lins, H. F.: USGS Hydro-Climatic Data Network 2009 (HCDN–2009): U.S. Geological Survey Fact Sheet 2012–3047, Tech. rep., US Geological Survey, Reston, VA, <https://pubs.usgs.gov/fs/2012/3047/>, 2012.
- Mason, S. J. and Graham, N. E.: Areas beneath the relative operating characteristics (ROC) and relative operating levels (ROL) curves: Statistical significance and interpretation, *Quarterly Journal of the Royal Meteorological Society*, 128, 2145–2166, <https://doi.org/10.1256/003590002320603584>, 2002.
- 840 MELCC: Données du Réseau de surveillance du climat du Québec, 2019.
- Mendoza, P. A., Wood, A. W., Clark, E., Rothwell, E., Clark, M. P., Nijssen, B., Brekke, L. D., and Arnold, J. R.: An intercomparison of approaches for improving operational seasonal streamflow forecasts, *Hydrol. Earth Syst. Sci.*, 21, 3915–3935, <https://doi.org/10.5194/hess-21-3915-2017>, 2017.
- Mortimer, C. and Vionnet, V.: Northern Hemisphere historical in-situ Snow Water Equivalent dataset (1979–2021),  
845 <https://doi.org/10.5281/ZENODO.10287092>, 2024.
- Mortimer, C., Mudryk, L., Derksen, C., Luojus, K., Brown, R., Kelly, R., and Tedesco, M.: Evaluation of long-term Northern Hemisphere snow water equivalent products, *The Cryosphere*, 14, 1579–1594, <https://doi.org/10.5194/tc-14-1579-2020>, 2020.
- Mortimer, C., Mudryk, L., Cho, E., Derksen, C., Brady, M., and Vuyvich, C.: Use of multiple reference data sources to cross validate gridded snow water equivalent products over North America, <https://doi.org/10.5194/egusphere-2023-3013>, 2024.
- 850 Musselman, K. N., Lehner, F., Ikeda, K., Clark, M. P., Prein, A. F., Liu, C., Barlage, M., and Rasmussen, R.: Projected increases and shifts in rain-on-snow flood risk over western North America, *Nature Climate Change*, 8, 808–812, <https://doi.org/10.1038/s41558-018-0236-4>, 2018.
- Pagano, T., Garen, D., and Sorooshian, S.: Evaluation of Official Western U.S. Seasonal Water Supply Outlooks, 1922–2002, *Journal of Hydrometeorology*, 5, 896–909, [https://doi.org/10.1175/1525-7541\(2004\)005<0896:EOWUS>2.0.CO;2](https://doi.org/10.1175/1525-7541(2004)005<0896:EOWUS>2.0.CO;2), 2004.
- 855 Painter, T. H., Berisford, D. F., Boardman, J. W., Bormann, K. J., Deems, J. S., Gehrke, F., Hedrick, A., Joyce, M., Laidlaw, R., Marks, D., Mattmann, C., McGurk, B., Ramirez, P., Richardson, M., Skiles, S. M., Seidel, F. C., and Winstral, A.: The Airborne Snow Observatory: Fusion of scanning lidar, imaging spectrometer, and physically-based modeling for mapping snow water equivalent and snow albedo, *Remote Sensing of Environment*, 184, 139–152, <https://doi.org/10.1016/j.rse.2016.06.018>, 2016.
- Renard, B., Kavetski, D., Kuczera, G., Thyer, M., and Franks, S. W.: Understanding predictive uncertainty in hydrologic modeling: The  
860 challenge of identifying input and structural errors, *Water Resources Research*, 46, <https://doi.org/10.1029/2009WR008328>, 2010.
- Shen, H., Tolson, B. A., and Mai, J.: Time to Update the Split-Sample Approach in Hydrological Model Calibration, *Water Resources Research*, 58, e2021WR031 523, <https://doi.org/10.1029/2021WR031523>, 2022.
- Slater, L. and Villarini, G.: Evaluating the Drivers of Seasonal Streamflow in the U.S. Midwest, *Water*, 9, 695, <https://doi.org/10.3390/w9090695>, 2017.
- 865 Slater, L. J., Arnal, L., Boucher, M.-A., Chang, A. Y.-Y., Moulds, S., Murphy, C., Nearing, G., Shalev, G., Shen, C., Speight, L., Villarini, G., Wilby, R. L., Wood, A., and Zappa, M.: Hybrid forecasting: blending climate predictions with AI models, *Hydrology and Earth System Sciences*, 27, 1865–1889, <https://doi.org/10.5194/hess-27-1865-2023>, 2023.
- Stagge, J. H., Rosenberg, D. E., Abdallah, A. M., Akbar, H., Attallah, N. A., and James, R.: Assessing data availability and research reproducibility in hydrology and water resources, *Scientific Data*, 6, 190 030, <https://doi.org/10.1038/sdata.2019.30>, 2019.
- 870 Sun, N., Yan, H., Wigmosta, M. S., Leung, L. R., Skaggs, R., and Hou, Z.: Regional Snow Parameters Estimation for Large-Domain Hydrological Applications in the Western United States, *Journal of Geophysical Research: Atmospheres*, 124, 5296–5313, <https://doi.org/10.1029/2018JD030140>, 2019.

- 875 Tang, G., Clark, M. P., Newman, A. J., Wood, A. W., Papalexiou, S. M., Vionnet, V., and Whitfield, P. H.: SCDNA: a serially complete precipitation and temperature dataset for North America from 1979 to 2018, *Earth System Science Data*, 12, 2381–2409, <https://doi.org/10.5194/essd-12-2381-2020>, 2020a.
- Tang, G., Clark, M. P., Newman, A. J., Wood, A. W., Papalexiou, S. M., Vionnet, V., and Whitfield, P. H.: SCDNA: a serially complete precipitation and temperature dataset in North America from 1979 to 2018 (Version 1.1), <https://doi.org/10.5281/ZENODO.3953310>, 2020b.
- 880 Tang, G., Clark, M. P., and Papalexiou, S. M.: SC-Earth: A Station-Based Serially Complete Earth Dataset from 1950 to 2019, *Journal of Climate*, 34, 6493–6511, <https://doi.org/10.1175/JCLI-D-21-0067.1>, 2021.
- USGS: USGS Water Data for the Nation, Natl. Water Inf. Syst. Web Interface, <https://waterdata.usgs.gov/nwis>, last accessed: 2023-12-05.
- Veiga, V., Hassan, Q., and He, J.: Development of Flow Forecasting Models in the Bow River at Calgary, Alberta, Canada, *Water*, 7, 99–115, <https://doi.org/10.3390/w7010099>, 2014.
- 885 Vionnet, V., Marsh, C. B., Menounos, B., Gascoïn, S., Wayand, N. E., Shea, J., Mukherjee, K., and Pomeroy, J. W.: Multi-scale snowdrift-permitting modelling of mountain snowpack, *The Cryosphere*, 15, 743–769, <https://doi.org/10.5194/tc-15-743-2021>, 2021a.
- Vionnet, V., Mortimer, C., Brady, M., Arnal, L., and Brown, R.: Canadian historical Snow Water Equivalent dataset (CanSWE, 1928–2020), *Earth System Science Data*, 13, 4603–4619, <https://doi.org/10.5194/essd-13-4603-2021>, 2021b.
- Vionnet, V., Mortimer, C., Brady, M., Arnal, L., and Brown, R.: Canadian historical Snow Water Equivalent dataset (CanSWE, 1928–2022), <https://doi.org/10.5281/ZENODO.7734616>, 2023.
- 890 Viviroli, D., Dürr, H. H., Messerli, B., Meybeck, M., and Weingartner, R.: Mountains of the world, water towers for humanity: Typology, mapping, and global significance: MOUNTAINS AS WATER TOWERS FOR HUMANITY, *Water Resources Research*, 43, <https://doi.org/10.1029/2006WR005653>, 2007.
- Wang, Q. J., Robertson, D. E., and Chiew, F. H. S.: A Bayesian joint probability modeling approach for seasonal forecasting of streamflows at multiple sites, *Water Resources Research*, 45, W05 407, <https://doi.org/10.1029/2008WR007355>, 2009.
- 895 Whitfield, P., Burn, D., Hannaford, J., Higgins, H., Hodgkins, G., Marsh, T., and Looser, U.: Hydrologic Reference Networks I. The Status of National Reference Hydrologic Networks for Detecting Trends and Future Directions, *Hydrological Sciences Journal*, 57, 1562–1579, <https://doi.org/10.1080/02626667.2012.728706>, 2012.
- Whitfield, P. H.: Is ‘Centre of Volume’ a robust indicator of changes in snowmelt timing?, *Hydrological Processes*, 27, 2691–2698, <https://doi.org/https://doi.org/10.1002/hyp.9817>, 2013.
- 900 Wood, A. W., Hopson, T., Newman, A., Brekke, L., Arnold, J., and Clark, M.: Quantifying Streamflow Forecast Skill Elasticity to Initial Condition and Climate Prediction Skill, *Journal of Hydrometeorology*, 17, 651–668, <https://doi.org/10.1175/JHM-D-14-0213.1>, 2016.
- Yan, H., Sun, N., Wigmosta, M., Skaggs, R., Hou, Z., and Leung, R.: Next-Generation Intensity-Duration-Frequency Curves for Hydrologic Design in Snow-Dominated Environments, *Water Resources Research*, 54, 1093–1108, <https://doi.org/10.1002/2017WR021290>, 2018.
- 905 Yuan, X., Wood, E. F., and Ma, Z.: A review on climate-model-based seasonal hydrologic forecasting: physical understanding and system development, *WIREs Water*, 2, 523–536, <https://doi.org/10.1002/wat2.1088>, 2015.
- Zamo, M. and Naveau, P.: Estimation of the Continuous Ranked Probability Score with Limited Information and Applications to Ensemble Weather Forecasts, *Mathematical Geosciences*, 50, 209–234, <https://doi.org/10.1007/s11004-017-9709-7>, 2018.
- Zhao, T., Schepen, A., and Wang, Q. J.: Ensemble forecasting of sub-seasonal to seasonal streamflow by a Bayesian joint probability modelling approach, *Journal of Hydrology*, 541, 839–849, <https://doi.org/10.1016/j.jhydrol.2016.07.040>, 2016.

910 Zheng, X., Wang, Q., Zhou, L., Sun, Q., and Li, Q.: Predictive Contributions of Snowmelt and Rainfall to Streamflow Variations in the Western United States, *Advances in Meteorology*, 2018, 1–14, <https://doi.org/10.1155/2018/3765098>, 2018.